8 Muon Trigger Introduction

8.1 Muon Detector

The CMS detector is a general purpose detector specifically optimized for muon measurement which is performed by Drift Tubes (DT) located outside of the magnet coil in the barrel region and Cathode Strips Chambers (CSC) in the forward region. The CMS Muon System is also equipped with Resistive Plate Chambers (RPC) dedicated for triggering. Positions of those three detectors are schematically shown in Fig. 8.1.

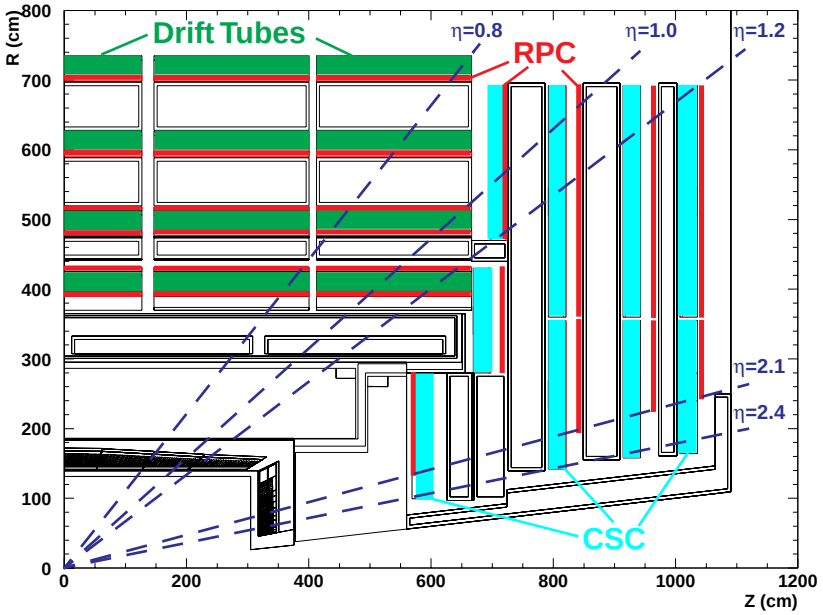

Fig. 8.1: Longitudinal cut of the CMS Muon System.

8.1.1 Drift Tubes

The layout of the barrel muon system [8.1] is shown in Fig. 8.2. It is composed of four muon stations interleaved with the iron of the yoke to make full use of the magnetic return flux (~1.8 T). This makes possible a muon momentum standalone measurement which is essential for the trigger and it is useful for the off-line matching of the muon reconstructed track to its image inside the inner tracker. The main drawback of a scheme with muon chambers packed close to the iron is the presence of an important electromagnetic background due to showering in the iron induced by muon bremsstrahlung, that complicates the track reconstruction. Together with the unavoidable cracks introduced for the supports and the cabling of large detectors, this background is the most important reason for the choice of an highly redundant design.

The redundancy is ensured by both number of stations and number of detector layers in each station. One station contains one or two RPC modules and one DT module. Each DT module is composed of three superlayers (SL) each one split in four layers of staggered drift tubes as shown in Fig. 8.3: two SL are measuring the coordinate in the bending plane (ϕ view) and one is looking at the longitudinal plane (θ view).

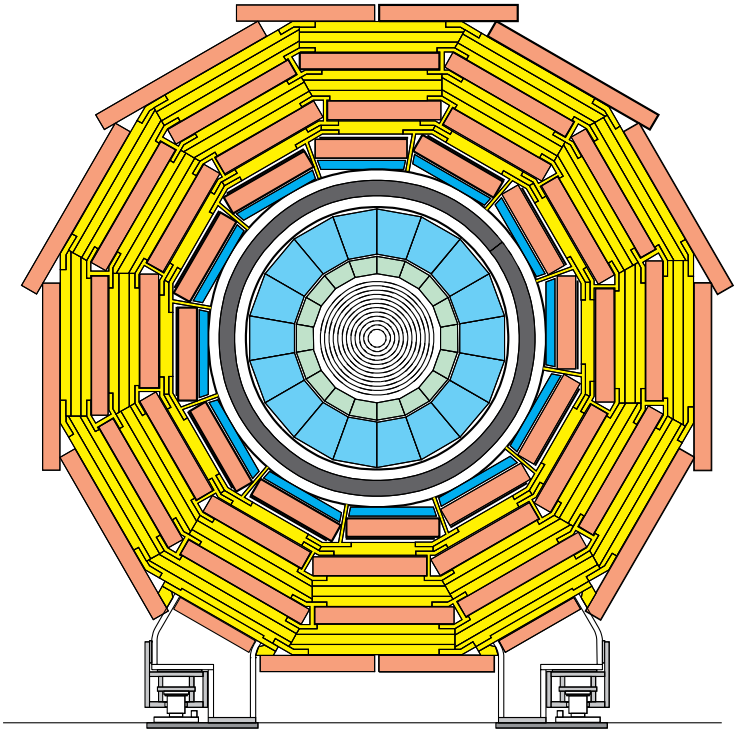

Fig. 8.2: Transverse view of the CMS detector.

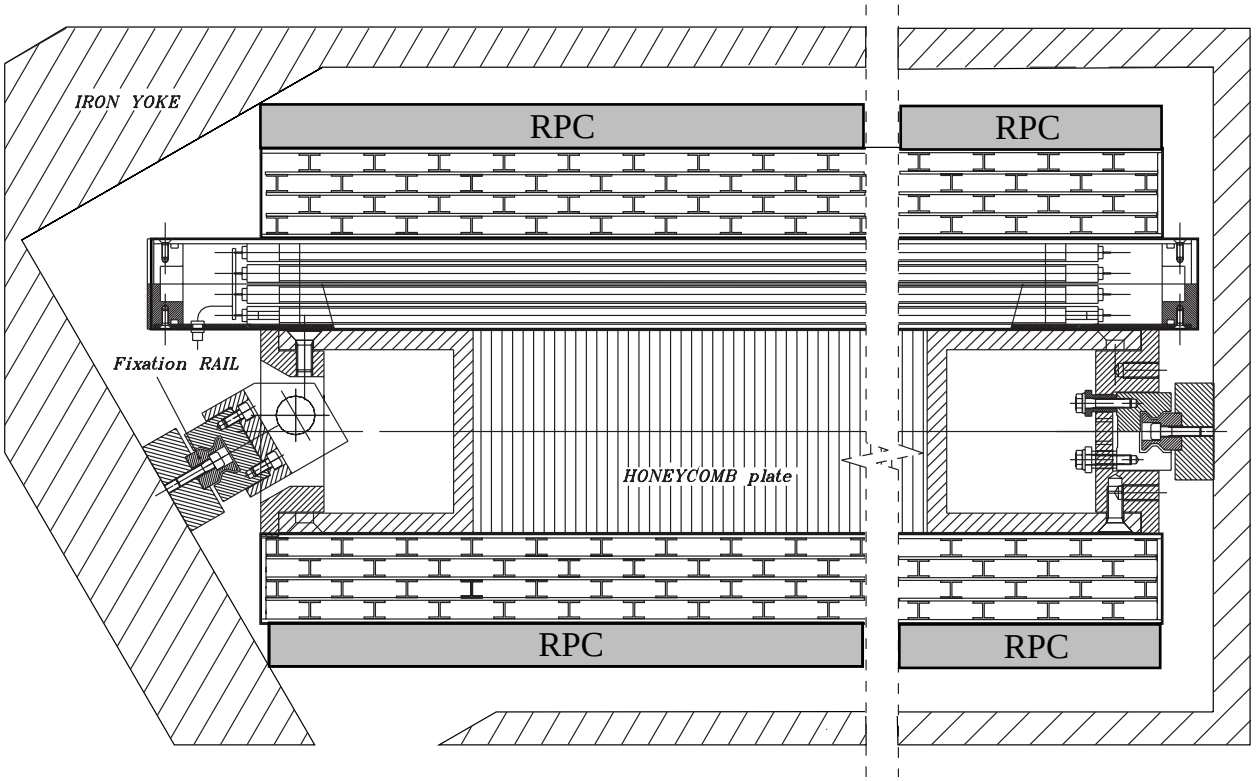

Fig. 8.3: Cross section of a barrel muon chamber.

The inner ϕ view SL is separated from the other ones by a 20 cm thick aluminum honeycomb plate that supplies the module with the required stiffness, permits the opening of an electromagnetic shower that can be generated inside the iron allowing a better measurement in the SL away from the iron and provides a lever arm in the bending plane useful for triggering purposes.

The outermost station differs from the inner ones, since it does not have a SL in the θ view. This SL is replaced by a honeycomb plate providing the same lever arm between the two ϕ view SLs. Its eventual contribution to the muon η assignment was found to be marginal.

The barrel chambers are drift chambers that are required to provide a final resolution of 100 μm per station and to be linear in the time to space conversion, i.e. to have a drift velocity constant along the whole drift path. Most of the past studies were therefore devoted to careful evaluation of the drift cell layout in order to meet these requirements. Several tests were done on a muon beam using various chamber prototypes [8.2][8.3]. The results of the tests fully matched the requirements.

8.1.2 Cathode Strip Chambers

Endcap muon stations are equipped with Cathode Strip Chambers (Fig. 8.4). CSCs are multiwire proportional chambers with segmented cathode readout. High precision coordinate along the wire is obtained by extrapolation of charges induced on several adjacent cathode strips. In CMS the strip width varies from 3.2 to 16 mm. Obtained resolution is in the range between 80 μm and 450 μm for one layer. For the trigger purposes, however, resolution of 1/2 of strip is good enough.

CMS chambers have trapezoidal shape. One chamber consists of six detecting layers. The layers are separated by 16 mm thick polycarbonate plastic honeycomb panels which make the chamber stiff and provide a lever arm necessary to measure angle of the tracks. In each layer the strips are running radially. In angular units the strip width $\Delta\phi$ varies from 2.0 to 4.3 mrad and the length $\Delta\eta$ from 0.35 to 0.60 η-units. Combined off-line resolution of six layers approaches 50 μm.

The wires are perpendicular to the strips, except ME1/1 where the wires are tilted by 25°. This is to compensate the Lorentz effect in high magnetic field (almost 4T) to which the chamber is exposed. The wires have 50 μm diameter and they are spaced by 2.5 or 3.175 mm. Groups of 5-17 wires are readout together providing the spatial resolution of ΔR = 16-54 mm, i.e. $\Delta\eta$ = 0.01-0.04.

8.1.3 Resistive Plate Chambers

RPC chambers are located both in the barrel and in the endcaps (Fig. 8.1). Each muon station is equipped with one RPC plane except the two innermost barrel stations 1 and 2 which contain two RPC planes (Fig. 8.3). This is because low momentum muons (p_T < 5-6 GeV/c) cannot reach the outer stations, for which a special low p_T trigger is foreseen. Such additional planes are not necessary in the endcaps where the same p_T corresponds to much higher total momentum. Thus, the low p_T reach of the CMS muon trigger is about 4 GeV/c in the barrel and 2.0-3.5 GeV/c in the endcaps. The RPC readout is segmented into strips 1-4 cm wide and 30-130 cm long. In the barrel the strips are running parallel to the beam, whereas in the endcaps they are radial. In angular units each strips covers $\Delta\phi$=(5/16)° and $\Delta\eta\approx$0.1.

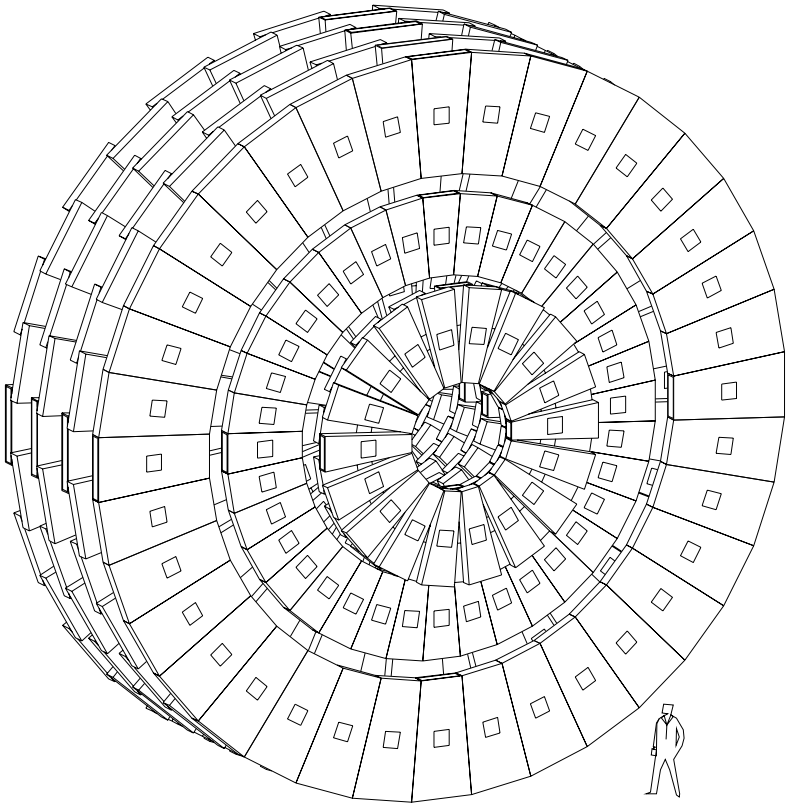

Fig. 8.4: Layout of the CMS Endcap.

8.1.4 Magnetic Field

Measurement of the muon transverse momentum p_T is based on track bending in the magnetic field. The magnetic field in the CMS detector is created by a long superconducting solenoid (Fig. 8.5). Since the dominant component of the $\boldsymbol{B}$ field is along the beam direction, tracks are primarily bent in the (r,ϕ) plane (perpendicular to the beam direction). Thus, tracks in (r,z) projection are approximately straight lines, i.e. they keep almost constant η value along the path. The presence of a radial field component $\boldsymbol{B_r}$, especially in the forward part of the detector, slightly modifies this picture. A track bent by the $\boldsymbol{p_T} \times \boldsymbol{B_z}$ force gets some tangential component p_ϕ. Then the $\boldsymbol{p_\phi} \times \boldsymbol{B_r}$ produces the z component of the Lorentz force. As a result, the track's η changes along its path. This deflection in η is rather small because the p_T component is small in comparison to the total p value. Even for the softest tracks reaching the muon stations, the change in η typically does not exceed 0.15 η-unit. Thus, in order to measure the transverse momentum of the track, it is enough to observe the dominant bending in the (r,ϕ) plane.

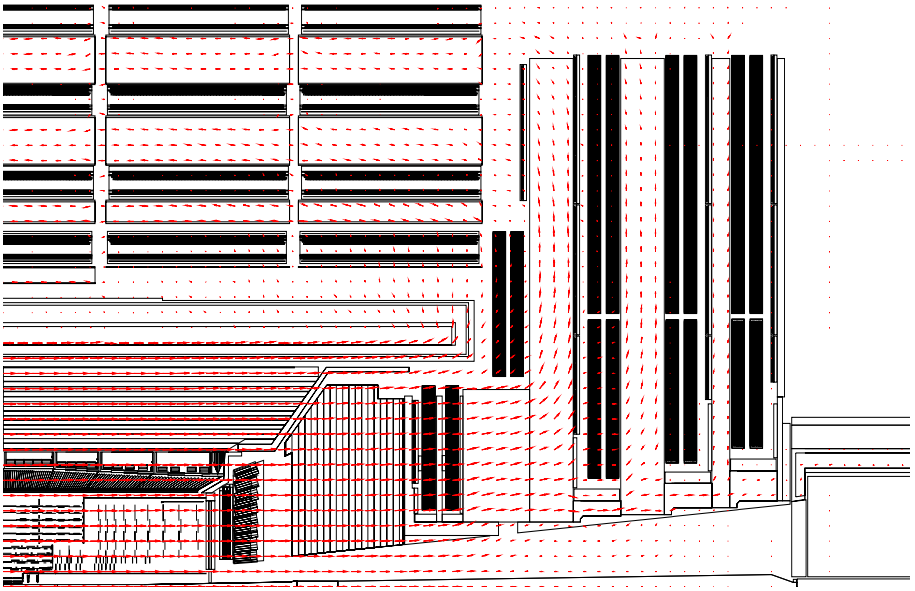

Fig. 8.5: CMS magnetic field map.

8.2 Muon Trigger Overall Structure

The First Level Muon Trigger of CMS uses all three kinds of muon detectors: Drift Tubes (DT), Cathode Strip Chambers (CSC) and Resistive Plate Chambers (RPC). The excellent spatial precision of DT and CSC ensures sharp momentum threshold. Their multilayer structure provides a possibility of effective background rejection. RPC are dedicated trigger detectors. Their superior time resolution ensures unambiguous bunch crossing identification. High granularity makes possible to work in high rate environment. Time information and both spatial coordinates of a detected particle are carried by the same signal, which eliminates ambiguities typical for wire detectors.

Complementary features of muon chambers (DT/CSC) and dedicated trigger detectors (RPC) allows us to build two trigger subsystems which deliver independent information about detected particles to the Global Muon Trigger. Advantages of having two such subsystems are numerous. The muon chambers and the dedicated trigger detectors deliver different information about particle tracks. They behave differently in difficult cases and they respond in different ways to various backgrounds. DT with long drift time (~400 ns) and CSC with charge weighting are more vulnerable to muon radiation for which RPC are much less sensitive. In the DT/CSC case, a background hit or track segment can eliminate the right one and cause some inefficiency. It is just the opposite in the RPC trigger processing all hits simultaneously, which may lead to some rate increase. Accidental coincidence of three of four background hits can be recognized by the RPC trigger as a real muon. This is very unlikely for DT/CSC as they look for coincidence of several planes in each station.

Properly combining the information from both systems results in high efficiency and powerful background rejection. Two extreme cases of such combinations would be the logical *OR*, which is optimized for efficiency, and the logical *AND*, optimized for background rejection. However, neither of these operations results in full use of the complementary functions of the

muon trigger components and a more sophisticated algorithm will be used. This is possible, because both the muon chambers and the dedicated trigger detectors deliver an information about the quality of detected muon candidates — number of hits in coincidence, matching between different chambers, etc. In general the muon candidate is taken in the two cases:

– it is seen by both RPC and DT/CSC subsystem (regardless of quality),

– it is seen by only one subsystem with high quality.

Another important advantage of the two component system is a possibility of crosschecks and cross calibration. Trigger data from the two components collected by the DAQ can be compared online. This enables the quick discovery of possible problems and gives a possibility of immediate action. When studying cross sections, asymmetries etc., it is very important to know the trigger efficiency and acceptance. Usually this is done by running with thresholds much lower than the measurement range. Two component system offers a unique ability to measure these quantities in a more unbiased way.

The muon trigger system consists of the following items:

– Drift Tube (DT) Trigger

– Cathode Strip Chamber (CSC) Trigger

– Pattern Comparator Trigger (PACT) based on Resistive Plate Chambers (RPC)

– Global Muon Trigger

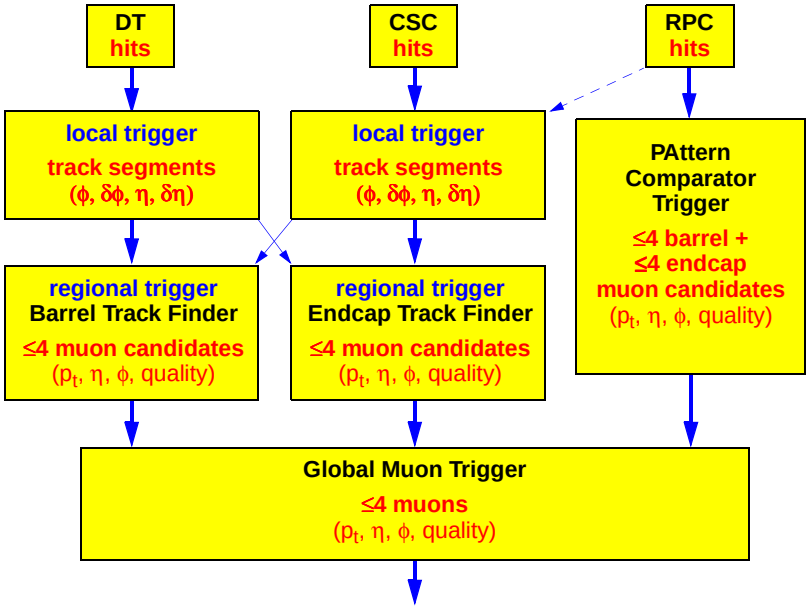

Fig. 8.6: Muon Trigger data flow.

Functional relations between the components are shown in Fig. 8.6. The data are exchanged between DT and CSC in the overlap region ($0.8<|\eta|<1.2$). In this way the Barrel Track Finder covers $|\eta|<1.0$, whereas the Endcap Track Finder covers $1.0<|\eta|<2.4$. Optionally, coarse RPC data can be sent to the CSC trigger in order to help solving spatial and temporal ambiguities in multimuon events.

The RPC trigger works on a grid of $\Delta\eta\times\Delta\phi = \sim 0.1 \times 2.5°$, which determines its two muon resolution. The DT and CSC triggers do not work on a fixed grid. The η and ϕ coordinates are calculated with precision of 0.05 η-unit and 2.5° respectively.

8.3 Algorithms and Implementation

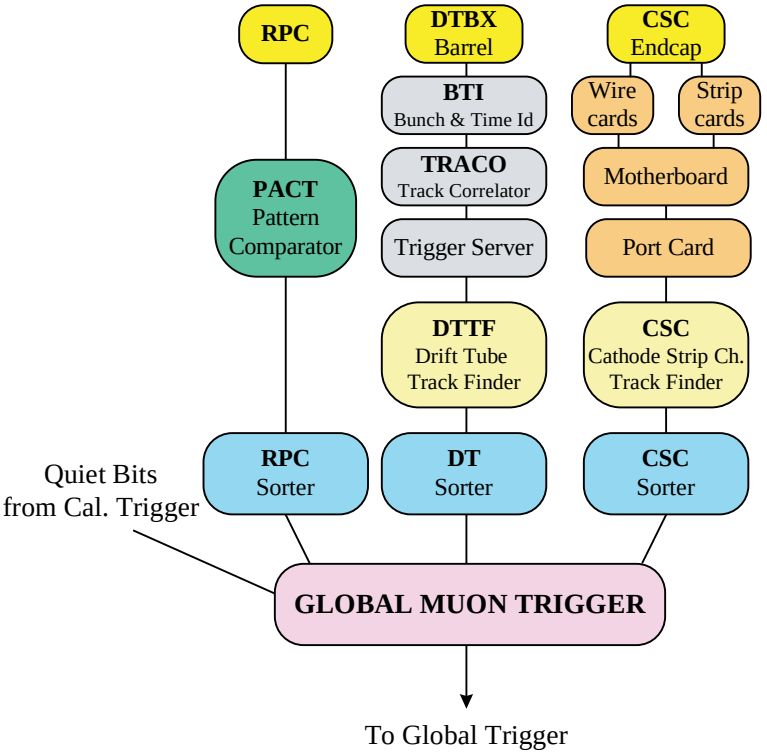

Fig. 8.7: Muon Trigger block diagram.

The logical structure of the Muon Trigger is shown in Fig. 8.7. DT and CSC electronics first process the information from each chamber locally. Therefore they are called *local triggers*. As a result one vector (position and angle) per muon per station is delivered. Vectors from different stations are collected by the Track Finder (TF) which combines them to form a muon track and assigns a transverse momentum value. TF plays the role of a *regional trigger*. Up to 4 best (highest p_T and quality) muon candidates from each system are selected and sent to the Global Muon Trigger.

In the case of RPC there is no local processing apart from synchronisation and cluster reduction. Hits from all stations are collected by PACT logic. If they are aligned along a possible muon track, a p_T value is assigned and the information is sent to the Muon Sorter. The Muon Sorter selects 4 highest p_T muons from the barrel and 4 from the endcaps and sends them to the Global Muon Trigger. The Global Muon Trigger compares the information from TF (DT/CSC) and PACT (RPC). So called quiet bits delivered by the Calorimeter Trigger are used to form an isolated muon trigger. The 4 highest p_T muons in the whole event are then transmitted to the Global Trigger. Finally transverse momentum thresholds are applied by the Global Trigger for all trigger conditions.

8.3.1 Drift Tube Trigger

The drift chambers deliver data for track reconstruction and triggering on different data paths. The local trigger is based on two SL in the ϕ view of the muon station. The trigger logical blocks are shown in Fig. 8.8.

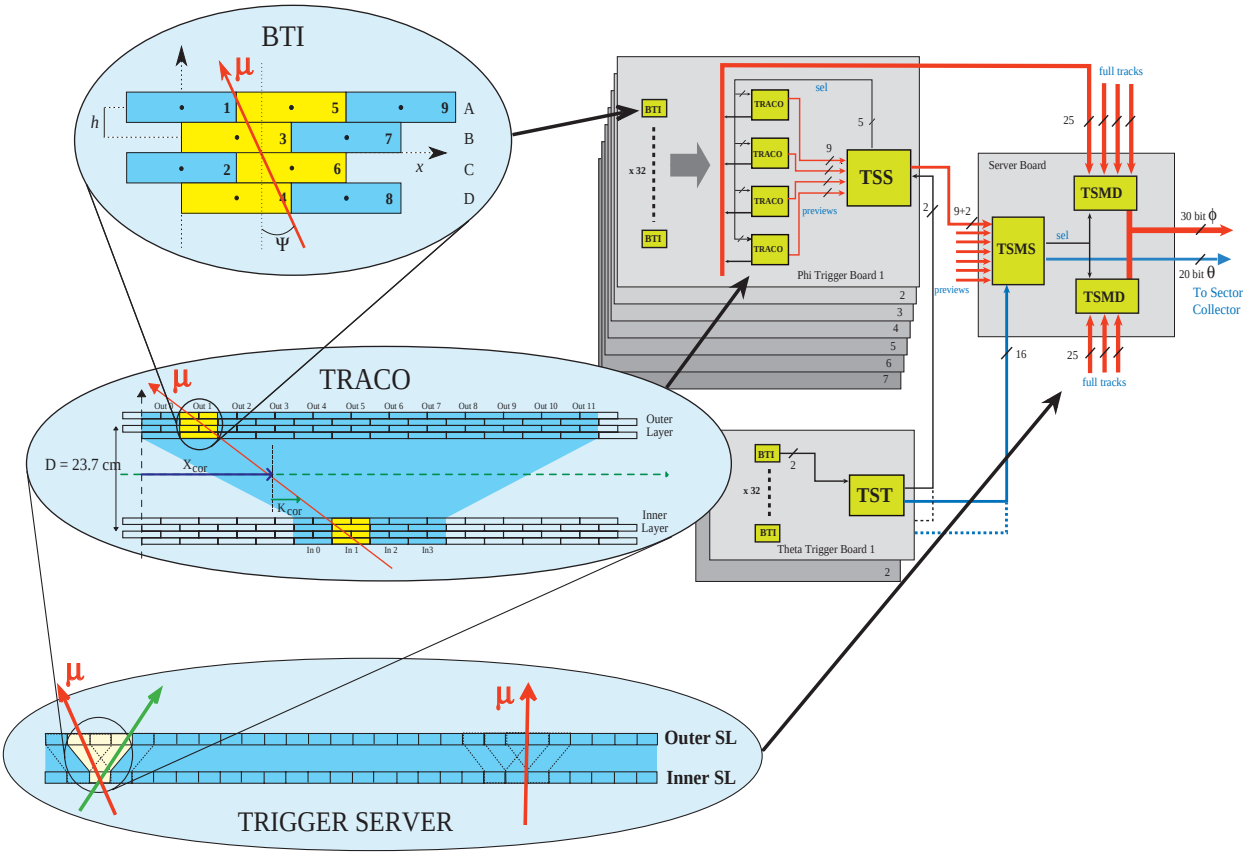

Fig. 8.8: Block scheme of the local trigger of a drift chamber.

The trigger front-end device, i.e. directly interfaced to the wire front-end readout electronics, is called Bunch and Track Identifier (BTI). It is used in the ϕ view and the θ view and performs a rough muon track fit in one station measuring position and direction of trigger candidate tracks with at least three hits, in different planes of a SL. The algorithm fits a straight line within programmable angular acceptance. Since it accepts three points tracks, the device is still working even if the drift time of a tube is missing, due to inefficiency, or wrong, due to the emission of a δ-ray, since there are still three useful cells giving the minimum requested information. It is also insensitive to all uncorrelated single hits. In the θ-view only tracks pointing to the vertex are selected. The BTI uses an internal resolution of 0.7 mm for its calculations, but the resolutions on the output parameters are ~1.4 mm on the impact position and ~60 mrad on the track direction.

This device performs the bunch crossing assignment of every found muon track candidate. The algorithm used in the device is a generalization of the mean-timer method [8.4].

Since this method must foresee alignment tolerances and needs to accept alignments of only three hits, the algorithm can generate false triggers. Hence in the bending plane a system composed by a Track Correlator (TRACO) and a chamber Trigger Server (TS) is used to filter the

information of the two ϕ SLs of a chamber in order to lower the trigger noise. The TRACO/TS block selects, at every cycle among the trigger candidates, at most two tracks with the smallest angular distances (i.e. higher p_T) with respect to the radial direction to the vertex.

In particular the TRACO improves the angular resolution of the muon candidate track to ~10 mrad using the larger lever arm available and is converting the triggering variables to p_T related quantities (the position in the detector as the angle ϕ and the bending angle ϕ_B), while the TS system is governing the two tracks selection decision and it is therefore deciding dimuon detection efficiency.

The TS outputs at most two track segments in cells of size $\Delta\phi \sim 1.5$ mrad and $\Delta\phi_B \sim 12$ mrad. This cell defines the minimal de facto separation between two segments necessary for their identification, although two identical objects are allowed on output. The η segmentation is variable along the detector, being at fixed z values: there are 40 pseudorapidity cells in the range $|\eta| \leq 1.2$.

Track segments found in each station are then transmitted to a regional trigger system called Drift Tube Track Finder (DTTF). The task of the Track Finder is to connect track segments delivered by the stations into a full track and assign a transverse momentum value to the finally resolved muon track [8.5][8.6][8.7]. The system is divided in sectors, each of them covering 30° in the ϕ angle. The Sector Processors are organized in twelve wedges along the η coordinate. The Sector Processors in the outermost barrel wheels receive track segment data also from the Cathode Strip Chambers system, in order to handle the overlap region track finding. Each Sector Processor is logically divided in three functional units - the Extrapolator Unit (EU), the Track Assembler (TA) and the Assignment Units (AU), as shown in Fig. 8.9.

The Extrapolator Unit attempts to match track segments pairs of distinct stations [8.5]. Using the spatial coordinate ϕ and the bending angle of the source segment, an extrapolated hit coordinate may be calculated. The match is considered successful if a target segment is found at the extrapolated coordinate, within a certain tolerance (see Fig. 8.9). Memory based look up tables are used in the calculation of the extrapolated hit coordinate and tolerance values. Since tracks may cross detector sector boundaries, the Extrapolator Unit can use the neighboring sector track segments as targets in the extrapolations [8.8]. The two best extrapolations per each source are forwarded to the Track Assembler.

The Track Assembler attempts to find at most two tracks in a detector sector with the highest rank, i.e. exhibiting the highest number of matching track segments and the highest extrapolation quality. This task is performed in three steps. First the Track Segment Linker joins the track segment pairs formed by the Extrapolation Unit to full tracks, which are then forwarded to the Track Selector unit. The Track Selector contains a cancellation logic that reduces the number of duplicated tracks. Finally it selects the two highest rank tracks. As a last step, the Address Assignment sub-unit extracts the corresponding track segment data from the data pipeline, and forwards them to the Assignment Unit.

Once the track segment data are available to the Assignment Unit, memory based look up tables are used to determine the transverse momentum, the ϕ and η coordinates, and a track quality. The transverse momentum is assigned using the difference in the spatial ϕ coordinate of the two innermost track segments. The ϕ coordinate is defined as the spatial coordinate of the track segment in the second muon station.

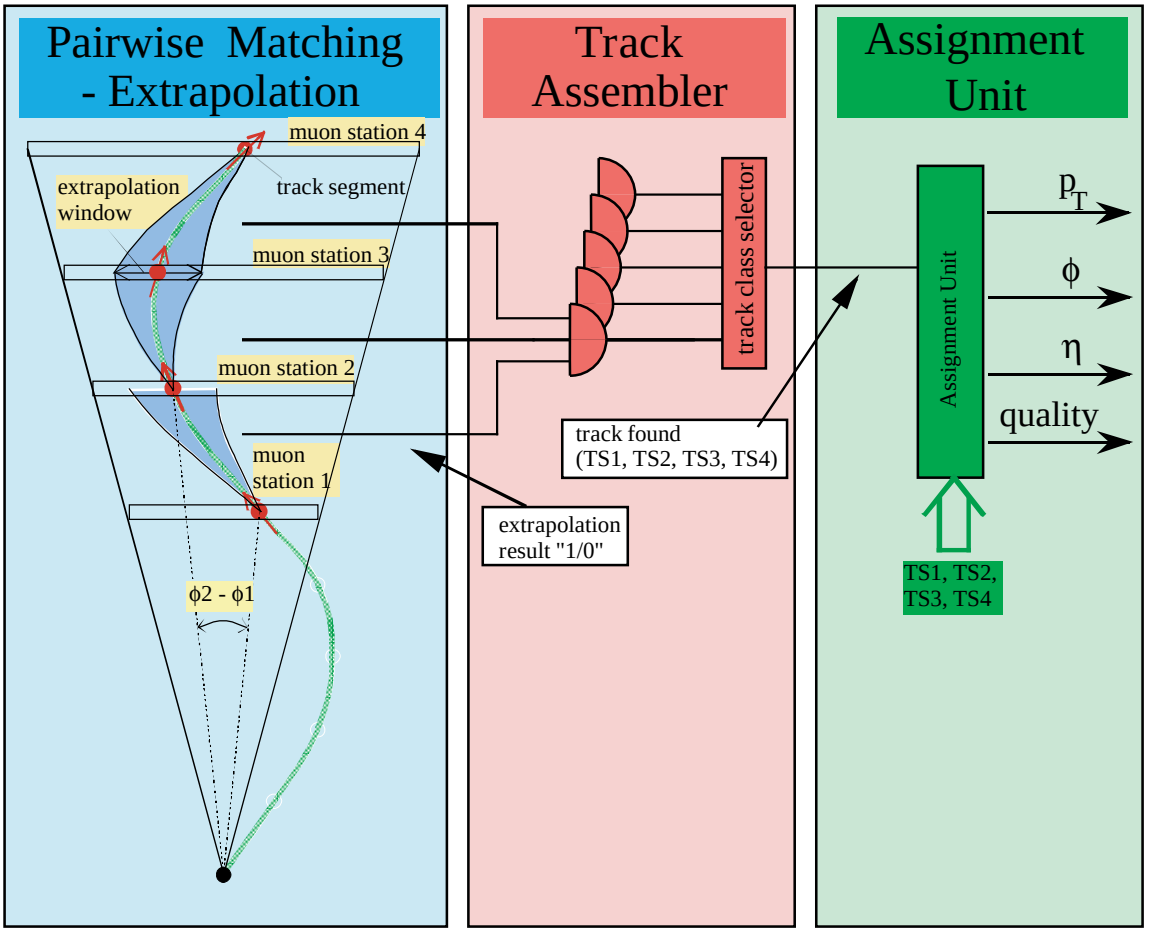

Fig. 8.9: Principle of the track finder algorithm (3-step scheme). On the left side, the pairwise matching algorithm is described. An extrapolated hit coordinate is calculated using the ϕ_1 coordinate and the bending angle of the source segment. The match is considered successful if a target segment is found at the extrapolated coordinate, inside a certain extrapolation window.

A preliminary coarse η assignment is derived from the place the track crossed detector wheel boundaries. A dedicated board has been designed for a finer η measurement; this measurement is derived by using the data from central Super Layers of the three innermost muon stations, which give a measurement of the *z*-coordinate of the track segments [8.9]. The η track finder board tries to match tracks along the η coordinate. At the Assignment step, the η track finder board attempts to match the found candidates with the ϕ Track Finder candidates. If the matching is successful, the fine η measurement is assigned to the Track Finder candidate, otherwise the coarse measurement is assigned.

Each Sector Processor forwards the two best ranking candidates to the Wedge Sorter, which selects the two track candidates with the highest transverse momentum. Each of the twelve Wedge Sorters sends the muon candidates to the Muon Sorter, which reduces the number of split tracks performing a check over the neighboring wedges candidates. The four highest momentum tracks are selected and then forwarded to the Global Muon Trigger for the final decision.

8.3.2 CSC Trigger

A block diagram of the CSC Trigger electronics is shown in Fig. 8.10. The task of the Cathode Strip Chamber (CSC) Track-Finder is to reconstruct tracks in the CSC endcap muon system and to measure the transverse momentum (p_T), pseudo-rapidity (η), and azimuthal angle (ϕ) of each muon. A p_T resolution of about 25% is necessary to have sufficient rate reduction at L1 with a reasonable threshold. The measurement of p_T by the CSC trigger uses spatial information from up to three stations to achieve a precision similar to that of the DT Track-Finder despite the reduced magnetic bending in the endcap. The CSC muon trigger finds muon candidates in the presence of large background rates from: low-energy photon interactions, where the photons originate from neutron-induced nuclear reactions; decay muons, especially at the lowest momenta and in the first muon station; punch-through pions, particularly in the first muon station; primary muons having low energy, and bremsstrahlung showers from the high-momentum muons themselves.

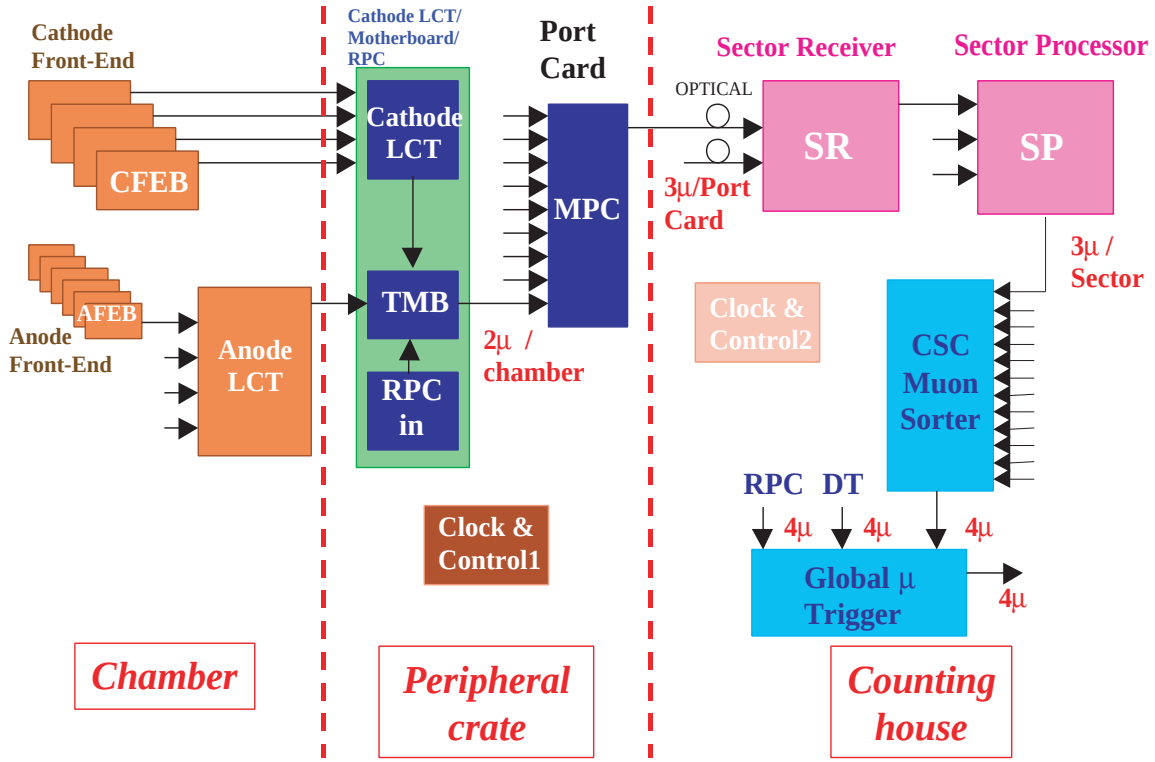

Fig. 8.10: Block diagram of the CSC Trigger.

At large rapidities, high backgrounds are expected from punch through pions, primary muons, secondary muons, and neutron-induced gamma rays. The high-rapidity muons also have higher momentum corresponding to a particular p_T and hence radiate more bremsstrahlung. The CSC Local Trigger provides high rejection power against these backgrounds by finding muon segments, also referred to as Local Charged Tracks (LCTs), in the 6-layer endcap muon CSC chambers. Muon segments are first found separately by anode and cathode electronics (see Fig. 8.11) and then time correlated, providing precision measurement of the bend coordinate position and angle, approximate measurement of the non-bend angle coordinate, and identification of the correct muon bunch crossing with high probability.

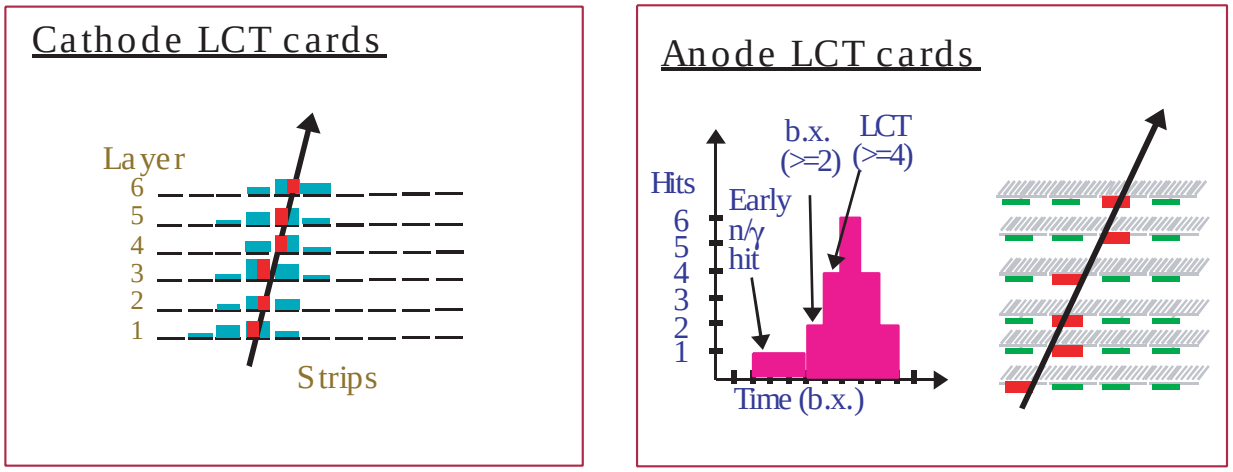

Fig. 8.11: Principle of the CSC Local Trigger.

The primary purpose of the CSC anode trigger electronics is to determine the exact muon bunch crossing with high efficiency. Within the CSC chambers, anode wires are hard-wired together or 'ganged' at the readout end in groups of 10-15 wires in order to reduce channel count. Anode signals are fed into amplifier/constant-fraction discriminators. Since the drift time can be longer than 50 ns, a multi-layer coincidence technique in the anode "Local Charged Track" (LCT) pattern circuitry is used to identify a muon pattern and find the bunch crossing. For each spatial pattern of anode hits, a low coincidence level, typically 2 layers, is used to establish timing, whereas a high coincidence level, typically 4 layers, is used to establish the existence of a muon track.

The primary purpose of the CSC cathode trigger electronics is to measure the ϕ coordinate precisely to allow a good muon momentum measurement up to high momentum. The charge collected on an anode wire produces an opposite-sign signal on several strips, and precision track measurement is obtained by charge digitization and precise interpolation of the cathode strip charges. A simpler and more robust method used by the CSC trigger achieves localization of the muon track to one-half of a strip width in each cathode layer. This is done with a 16-channel "comparator" ASIC that inputs amplified and shaped signals and compares the charges on all adjacent and next-to-adjacent strips. If a strip charge is found to be larger than those on its neighbors, a hit is assigned to the strip. Simultaneous comparison of left versus right neighbor strip charges allows assignment of the hit to the right or left side of the central strip, effectively doubling the resolution. The six layers are then brought into coincidence in LCT pattern circuitry to establish position of the muon to an RMS accuracy of 0.15 strip widths. Strip widths range from 6-16 mm.

Cathode and anode segments are brought into coincidence and sent to CSC Track Finder electronics which links the segments from the endcap muon stations. Each Track Finder unit finds muon tracks in a 60^{o} sector. Because of the limited bending in the endcap region, information is not shared across sector boundaries. Each CSC Track Finder can find up to three muon candidates. A CSC muon sorter module selects the four best CSC muon candidates and sends them to the Global Muon Trigger.

8.3.3 RPC Trigger

The algorithm behind the RPC based Pattern Comparator Trigger has been described in detail elsewhere [8.10]. Here, we would like to recall its salient features and make some general comments on practical implementation, which is described in details in Chapter 13.

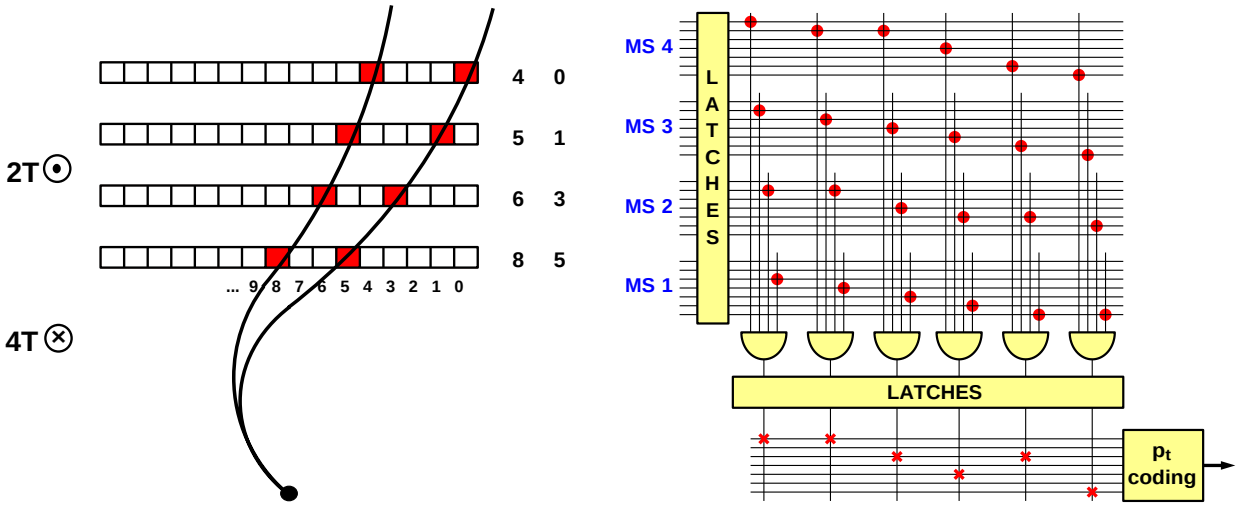

Fig. 8.12: RPC Trigger principle.

The algorithm

PACT is based on the spatial and time coincidence of hits in four RPC muon stations (see Fig. 8.12). We shall call such a coincidence a candidate track or a hit pattern. Because of energy loss fluctuations and multiple scattering there are many possible hit patterns in the RPC muon stations for a muon track of defined transverse momentum emitted in a certain direction. Therefore, the PACT should recognize many spatial patterns of hits for a given transverse momentum muon. In order to trigger on a particular hit pattern in the RPCs left by a muon, the PACT electronics performs two functions: requires time coincidence of hits in at least 3-out-of-4 muon stations (so called 3/4 candidate; better is 4/4 one) along a certain road and assigns a p_T value. The coincidence gives the bunch crossing assignment for a candidate track. The candidate track is formed by a pattern of hits that matches with one of many possible patterns pre-defined for muons with defined transverse momenta. The p_T value is thus given. The pre-defined patterns of hits have to be mutually exclusive i.e. a pattern should have a unique transverse momentum assignment. The patterns are divided into classes with a transverse momentum value assigned to each of them. PACT is a threshold trigger; it gives a momentum code if an actual hit pattern is straighter than any of pre-defined patterns with a lower momentum code. The patterns will depend on the direction of a muon i.e. on ϕ and η.

The number of patterns for a low transverse momentum muon track might be huge. Fortunately, for these strongly bent tracks we do not need full granularity of RPCs and can reduce the number of patterns by suitably OR-ing RPC strips on the PACT input. In fact, one can adapt granularity for different p_T values, using full one for straight hit patterns and progressively OR-ed ones for more curved hit patterns. This is the idea of dynamic cone on which the current PAttern Comparator (PAC) processor - a kernel of PACT- is based. This concept has the advantage of moderate number of patterns per track (80 in the current design) and manageable number of input strips to a PAC.

Segmentation of PACT

Ideally, the RPC geometry should be projective in ϕ; the strip width vary from 10 mm at high $|\eta|$ and low radii to about 40 mm at the outer radius of CMS. In reality, the RPC azimuthal symmetry is broken (see e.g. Fig. 8.2) in a different way for every station in the barrel. This leads to the dependence of pre-defined pattern on ϕ mentioned above. The logical segmentation is defined uniquely in so called reference station, which for most of the detector is Muon Station 2. The segmentation in ϕ is based on the basic PACT logical unit called segment. Every segment subtends 2.5° in ϕ i.e. 8 RPC strips in the reference station, and is serviced by one PAC processor. In non-reference stations more strips are connected forming a cone. The cones from neighbouring segments overlap. While the assignment of strips in the reference station to a segment and its PAC is unique, the strips in non-reference stations are connected to several segments, hence the need to split the RPC strip signals to several destinations.

The PACT is segmented in η into 33 towers, each covering roughly $\Delta\eta \approx 0.1$. This does not coincide with physical segmentation of the RPCs. Hence the need of OR-ing the strip signals from different chambers, and overlapping cones in η for segment processors. Each segment i.e. each PAC processor finds at most one candidate track. Internally, there may be several candidates found by a PAC inside one segment. The best candidate (i.e. with the best quality and then the highest transverse momentum) is selected and its momentum code, muon charge and quality bits are sent to PAC output.

Ghosts, ghost-busting and sorting

One of the requirements for the RPC Muon Trigger is to deliver the 4 highest transverse momentum muon candidates in the barrel and 4 in two endcaps. This means that we need to sort the list of candidates for barrel and endcaps to find the highest ones. Before any sorting, however, we have to reduce the number of ghosts. There are cracks in geometrical coverage of the RPCs due to gaps between CMS barrel wheels as well as to the gaps between RPCs in a given muon station. In order to maximize the efficiency the PACT accepts not only 4/4 but also 3/4 candidate tracks and uses overlapping cones as inputs to PACs. This causes appearance of ghosts i.e. candidate tracks in neighbouring segments in ϕ and/or η. Simulation shows that, typically, ghosts in ϕ are 3/4 candidates with higher p_T than the real 4/4 candidate tracks. They could increase significantly the trigger rate and we have to suppress them before sorting. There are two ghost-busting (GB) engines implemented in PACT: one for GB in ϕ, just after the layer of PAC processors, the second after sorting in one trigger tower (144 PACs). After last GB in η, there is final sorting to be done before producing up to 4+4 final candidates in barrel and endcaps.

8.3.4 Global Muon Trigger

The choice to have two separate muon systems was one of the determining ideas in the concept of the CMS detector. The basic design goals were excellent efficiency and control of trigger rates as well as redundancy. The Global Muon Trigger achieves the first two goals by choosing muon parameters from the most suitable system. Redundancy is achieved by the fact that the GMT can also use only one system in case of deficiency of the other. Special attention is given to ghost suppression, i.e. to the correct identification of identical muons seen twice.

The Regional Muon Trigger reconstructs muon candidates in both the barrel and the endcap regions out of hits or track segments found at the muon stations. For RPCs this is the Pattern

Comparator Trigger (PACT) covering the entire η-region. The DTs and CSCs have separate track finders. The GMT receives the best four barrel DT and the best four endcap CSC muons and combines them with 4+4 muons sent by the RPC PACT. It performs a matching based on the proximity of the candidates in (η,ϕ) space. If two muons are matched their parameters are combined to give optimum precision. If a muon candidate cannot be confirmed by the complementary system quality criteria can be applied to decide whether to forward it. The muon candidates are ranked based on their transverse momentum, quality and to some extent pseudorapidity and the best four muon candidates in the entire CMS detector are sent to the Global Trigger.

The Global Muon Trigger also receives information from the calorimeters. The Regional Calorimeter Trigger sends two bits based on energy measurements representing isolation and compatibility with a minimum ionizing particle in $\Delta\eta \times \Delta\phi = 0.35 \times 0.35$ trigger regions. The GMT extrapolates the muon tracks back to the calorimeter trigger towers and appends the corresponding ISO (isolation) and MIP (minimum ionizing particle) bits to the track data consisting of p_T, sign of the charge, η, ϕ and quality.

The GMT hardware consists of two GMT logic boards located in the Global Trigger crate. There is no separate crate for the GMT. Before the calculations can be done the incoming data from the different muon detectors and the calorimeter bits have to be aligned in time to each other and to the LHC bunch crossing structure. For the calorimeter MIP and ISO bits this is done on separate Pipeline Synchronizing Buffer modules also located in the Global Trigger crate which send the information to the GMT logic boards via the backplane. The four output muons are sent to the Global Trigger via the backplane.

8.4 Summary of Algorithm Performance

8.4.1 Simulation Tools

All the results presented in this section were obtained with PYTHIA [8.11] event generator. Trigger rates were calculated using large samples containing about 10^7 "minimum bias" single-muon and di-muon events and $4 \cdot 10^6$ W, Z and Drell-Yan events. Details are described in [8.12].

Particle passage through the detector was simulated with CMSIM [8.13] program based on GEANT 3 package [8.14]. The only exception is the neutron background simulation which was performed by a stand alone version of FLUKA [8.15] with proper simulation of thermal neutrons. In order to properly simulate punch-through effects the hadronic interactions were switched on. Muons were enabled to produce delta-rays, bremsstrahlung photons and e^+e^- pairs.

The detector response was simulated with ORCA [8.16] program, unless otherwise stated. It contains detailed description of the trigger hardware mapped into the object oriented structure in such a way that each board (in some cases a chip) is represented by a C++ object. The algorithms are simulated using bit-wise arithmetic.

8.4.2 Background

The task of the Muon Trigger is difficult because of the presence of severe background. In fact this is the major challenge of the design. There are three main sources of background:

- proton-proton interactions themselves,
- beam losses because of the limited LHC aperture (p-nucleus collision with energy of 7 TeV in the laboratory system),
- cosmic rays.

These sources produce various effects in the detectors. We group them into four classes depending on how they can influence the trigger:

track — a set of aligned track segments from several muon stations,

track segment — a set of aligned hits within one muon station,

correlated hit — caused by a genuine muon or its secondaries,

uncorrelated hit — caused by phenomenon not related to a given muon.

Dominant sources of each class of background are given in Table 8.1.

Table 8.1: Background classification.

detected objects	caused by	dominant source
tracks	low p_T muons	b- and c-quark decays, π and K decays
track segments	hadrons	punch-through and back-splashes
correlated hits	electrons	muon bremsstrahlung, δ-rays, e^+e^- production
uncorrelated hits	electrons	thermal neutrons $\rightarrow \gamma \rightarrow$ e

Muons

Muons come from several sources:

1. Proton-proton interactions
   (a) decays of heavy objects like W, Z, top, higgs, etc.,
   (b) b- and c- quark decays,
   (c) decays of hadrons composed with quarks u, d and s (mainly π and K),
   (d) punch-through of hadronic showers.
2. Beam losses because of the limited LHC aperture (sometimes called *beam halo muons*).
3. Cosmic rays.

The most difficult background is genuine low p_T muons. It is difficult to distinguish soft punch-through muons from other charged particles produced in hadronic showers. Therefore, we will discuss them together with punch-through hadrons.

Muons of type 1a and 1b together are often called **prompt muons**, because they are produced very close to the pp vertex. The life time of the longest living b-mesons, expressed as $c\tau$, is no longer than 500 μm. Even taking into account the relativistic dilation most of the particles containing b or c quark will decay within 1 cm from the vertex. The decays of b- and c-quarks dominate the rate of prompt muons (see Fig. 2.4, where b and c decays are included in the "minimum bias" set).

Prompt muons dominates the overall muon rate except for very low p_T (< 5 GeV/c) where **muons from π and K decays** become more important, as shown in Fig. 8.13.

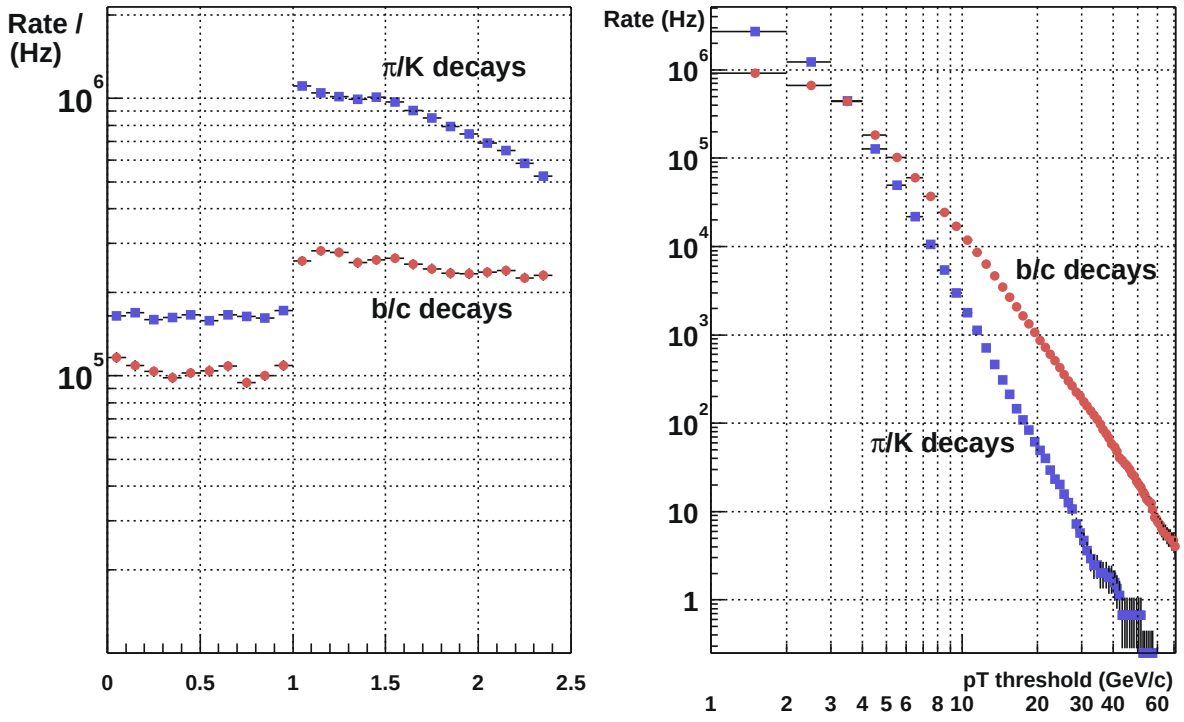

Fig. 8.13: Rates of muons entering the Muon System.

A typical rate of **cosmic muons** on the ground level is about 200 Hz/m^2. One can expect a reduction factor of approximately one hundred with respect to ground level cosmic rate. Hence the local rate is ~2 Hz/m^2 and it is completely negligible compared to other sources. Since the detector cross section has roughly 22×15 m^2 the total rate of cosmic muons crossing it is about 700 Hz. Only very few of the cosmic muons will have a chance to give a trigger because it requires the tracks to be pointing to the vertex. Most of them will create only very low p_T, poor quality track segments.

Beam halo muons. The limited aperture of the LHC causes some beam losses. Particles deviating from the beam center will interact with machine elements producing many secondaries. Most dangerous of them are energetic muons because of their ability to penetrate matter. They will enter the experimental hall and traverse the detector almost parallel to the beam. They have a very small probability to cause the trigger because they do not point to the vertex. In the endcap

chambers, however, they might be seen as local track segments. Estimated rate of halo muons varies from 10^{-2} Hz/cm^2 to 1 Hz/cm^2 depending on the distance from the beam.

The **total rate of muon hits** is shown in Fig. 8.14 as a solid line. It is a sum of all contributions discussed above.

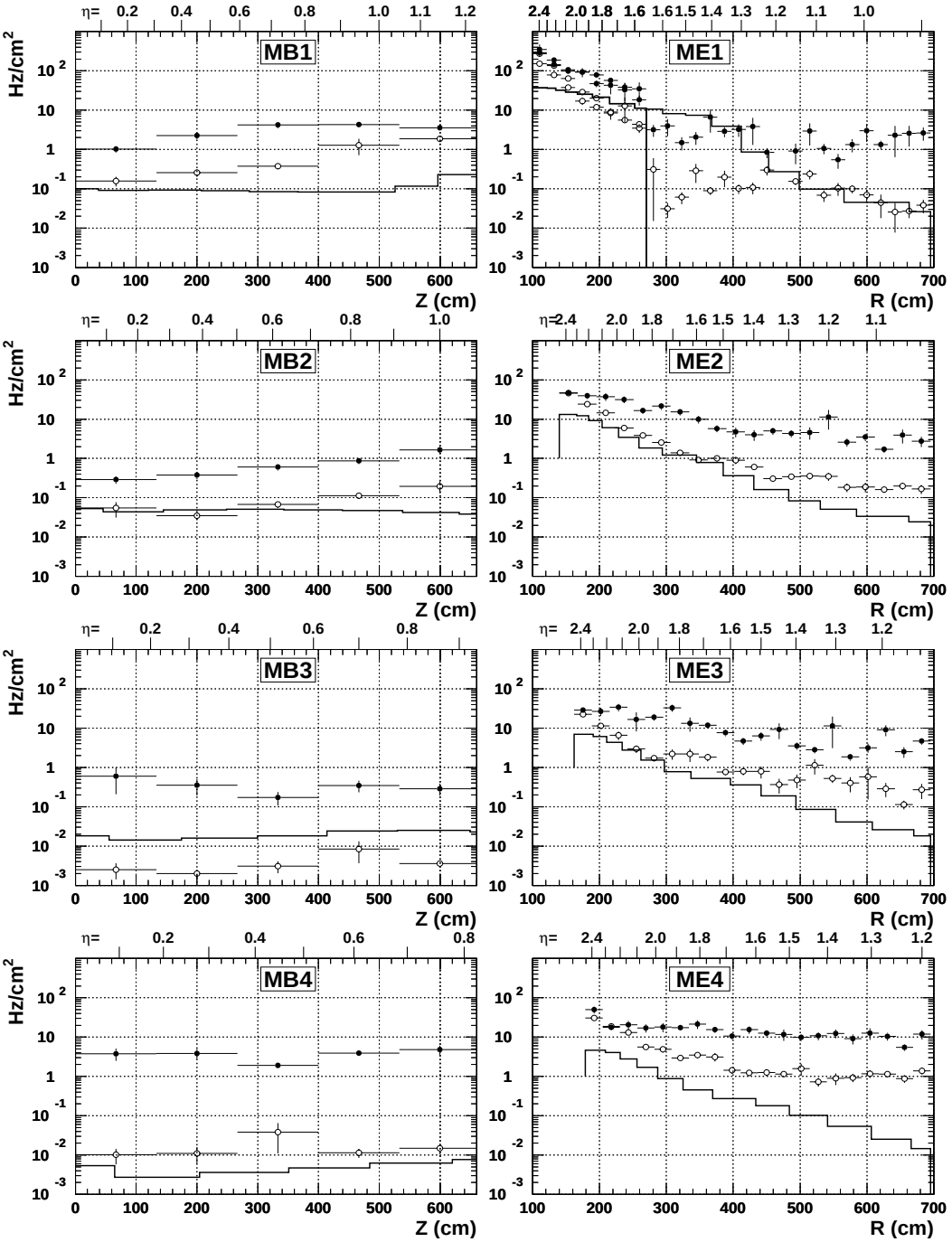

Fig. 8.14: Hit rates in muon chambers due to muons (solid line), hadronic punchthough/backsplashes (open circles) and thermal neutrons (full circles).

Hadrons

punch-through. The thickness of the CMS calorimeters varies from 11 to 15 interaction lengths λ. This is enough to contain most of hadronic showers caused by energetic hadrons. However, in some cases particles from the tails of the showers may enter muon detectors. This phenomenon was extensively studied experimentaly in the early stage of the LHC R&D in a dedicated experiment RD5 [8.17]. The results were used to tune Monte Carlo simulations.

When highly energetic hadron hits one of the forward detector elements some products of the hadronic shower can be emitted at large angles and travel towards muon chambers. This effect is often called a **backsplash**, although it has very similar nature to punch-through and the division is somewhat artificial. The total rate of charged hadrons due to punch-through and backsplashes of particles from pp interactions is shown in Fig. 8.14 as open circles.

Uncorrelated electrons from neutrons ("neutron background")

The very last product of hadronic showers are thermal neutrons. They cannot cause hits in detectors by themselves. However, they can be captured by nuclei and produce photons by deexcitation. Such a photon can in turn create an e^+e^- pair eventually causing hits in detectors. If the capture happens in iron or hydrogen the photons have energy of 2-8 MeV which may result in electrons penetrating several chamber layers. For rough estimates, one can assume that the flux of electrons causing hits is ~100 times lower than the photon flux, which is in turn ~10 times lower than the flux of neutrons. The thermal neutrons behave like a gas filling all the experimental hall. They can travel long distances even in dense matter and therefore it is difficult to shield them out.

There is another mechanism through which neutrons can produce detector hits. Elastic neutron-proton collision can give some kinetic energy to the proton which can be then registered by the detector. It has been shown [8.18], however, that the hit rate due to this effect is negligible compared to the $n \rightarrow \gamma \rightarrow e$ mechanism. The total rate of hits due to neutrons is shown in Fig. 8.14 as full circles.

Electrons correlated with muons ("muon radiation")

Muon traversing matter can lose its energy by four processes

- ionization (including delta ray production),
- bremsstrahlung, i.e. photon emission,
- direct e^+e^- pair production,
- nuclear interactions.

Probability of the last one can be neglected compared to others. Probability of the first three processes is given in Fig. 8.15 as a function of muon momentum and energy of secondaries. The most probable effect is an emission of a soft delta ray. Probability of hard (> 1 GeV/c) electron or photon emission is relatively low, but such particle usually develops entire electromagnetic shower which can disturb seriously the muon measurement. Probability of such shower in one of four muon stations is about few percent for muons above 100 GeV/c and it exceeds 10 % for 1 TeV/c muons.

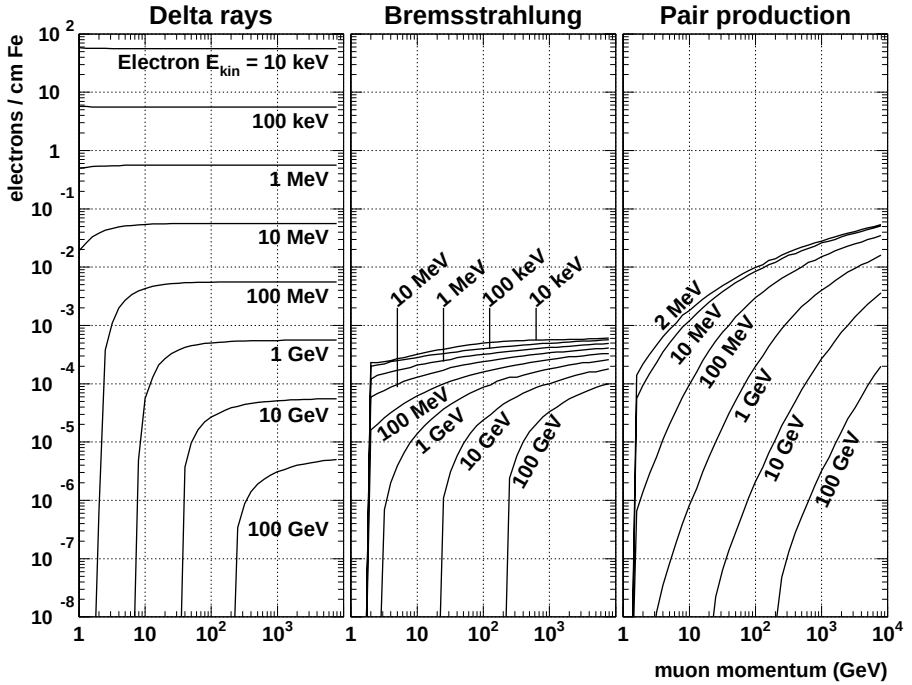

Fig. 8.15: Production of electrons by muons traversing iron [8.14].

8.4.3 Muon isolation

Muons from decays of heavy objects (W and Z bosons, SUSY higgses A, H and h, etc.) are usually isolated, whereas those from quark decays are accompanied by jets. One can improve signal to background ratio by vetoing muons surrounded by significant energy deposit in calorimeters. Muons can be tagged as “isolated” or “nonisolated” by the Global Muon Trigger using quiet bits from the Calorimeter Trigger. One quiet bit is associated with a calorimeter region of $\Delta\eta \times \Delta\phi = 0.35 \times 0.35$. This is usually too small to contain full energy of a jet. Therefore isolation algorithms based on larger area were also studied — 1×2, 2×2 and 3×3 regions. A muon was considered isolated if the entire area of the sliding window centered on the muon was quiet. Two signal examples were chosen: an inclusive $W \rightarrow \mu$ sample and $A \rightarrow \mu\mu$ sample. Background was represented by $b\bar{b}$ pairs. The simulation was done with Pythia/CMSIM, with and without pileup in order to study low and high luminosity cases [8.19]. Only the barrel ($|\eta|<1$) was considered.

Efficiency of single isolated muon trigger for signal and background is shown in Fig. 8.16 as a function on the quality bit threshold E_T. On the basis of this figure the E_T threshold was set to ensure 90 % efficiency for muons from A higgs decays. It corresponds to 95 % or higher efficiency for muons from W. Selected E_T values are given in Table 8.2. The efficiency for background muons is shown in Fig. 8.17 as a function of muon p_T threshold.

It is seen that the isolation is not very effective for low p_T muons. This is because they are usually accompanied by soft, wide jets with energy per region less then the isolation threshold. The isolation becomes effective for muons with p_T >15 GeV/c. At low luminosity 2×2 and 3×3 algorithms give equally good results. At high luminosity the 2x2 algorithm is the best. More details can be found in Ref. [8.19].

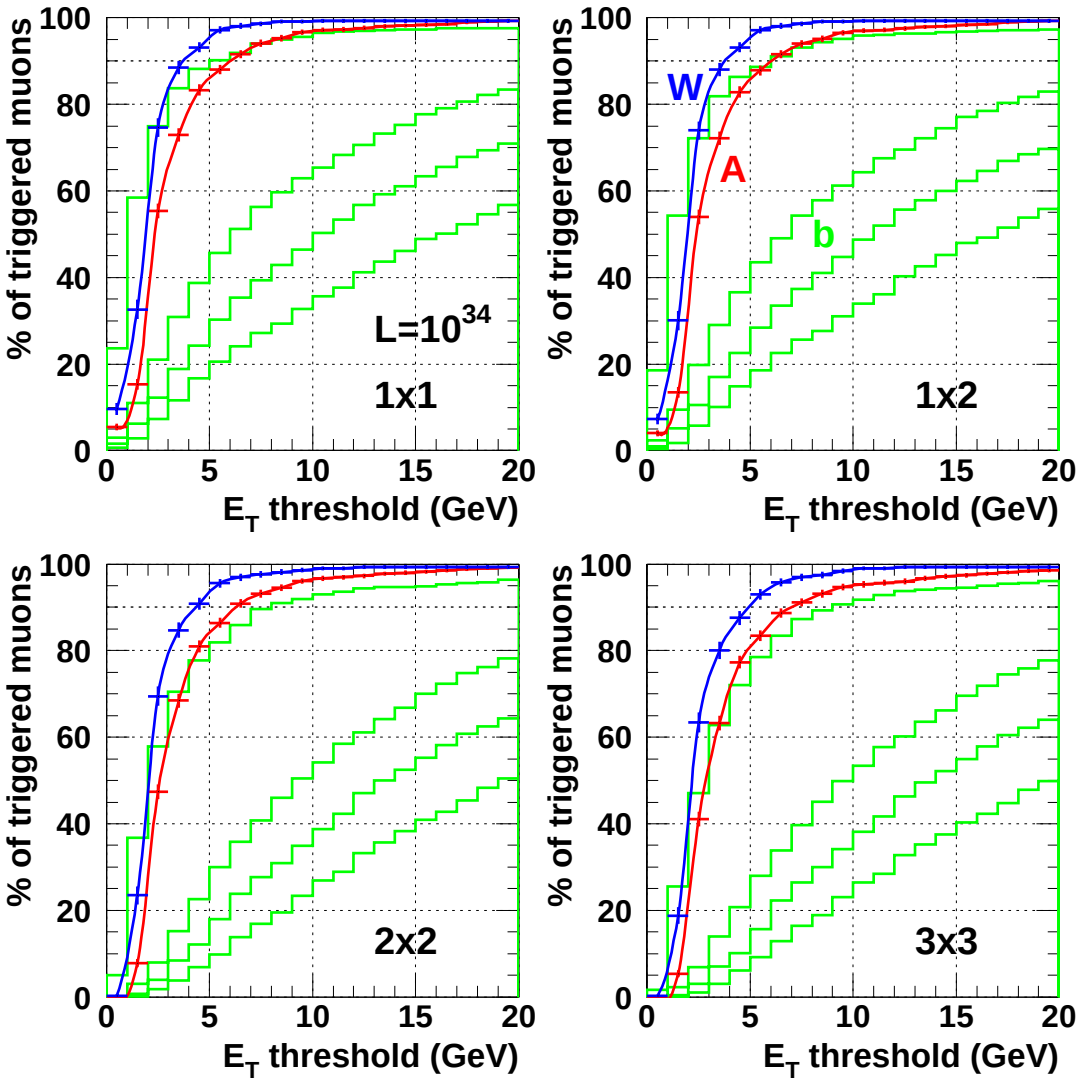

Fig. 8.16: Fraction of accepted events as a function of energy threshold at high luminosity. The upper and lower curves with error bars represent the W and A^0 signal respectively. The four histograms in each plot correspond to muons from b-quark decays with $p_T > 5$ (the upermost), 15, 20 and 25 GeV/c.

Table 8.2: Muon isolation thresholds E_T for different algorithms.

algorithm	$\Delta\eta \times \Delta\phi$	E_T for 10^{33} cm^{-2} s^{-1}	E_T for 10^{34} cm^{-2} s^{-1}
1×1	0.35×0.35	6 GeV	7 GeV
1×2	0.35×0.70	6 GeV	7 GeV
2×2	0.70×0.70	6 GeV	7 GeV
3×3	1.05×1.05	7 GeV	8 GeV

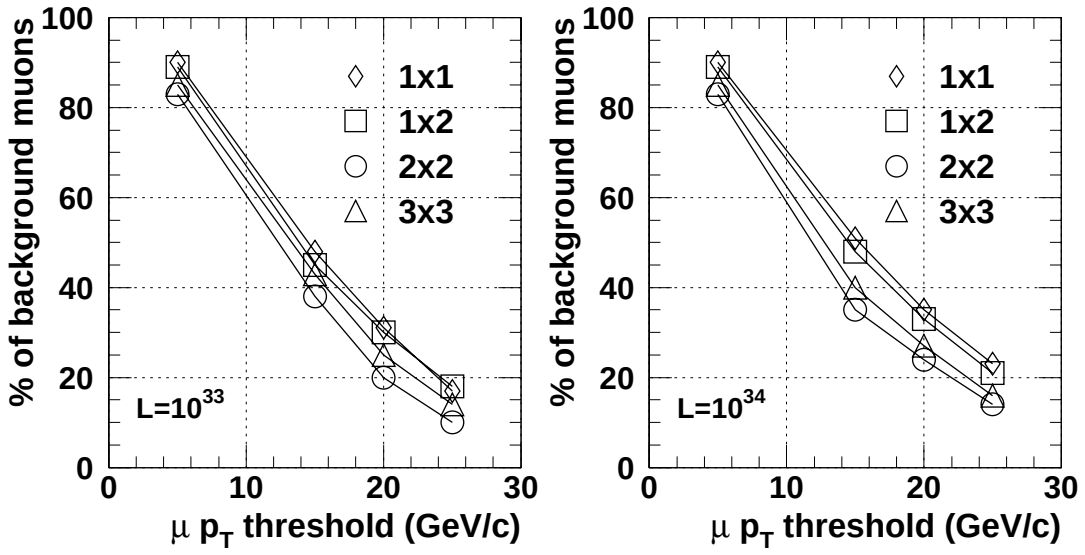

Fig. 8.17: Single isolated muon trigger efficiency for background ($b\bar{b}$) muons.

8.4.4 Trigger efficiency and rates

The Muon Trigger performance was tested using tools described in Section 8.4.1. Simulated efficiency is shown in Fig. 8.18 as a function of η. It is seen that it exceeds well 95 %.

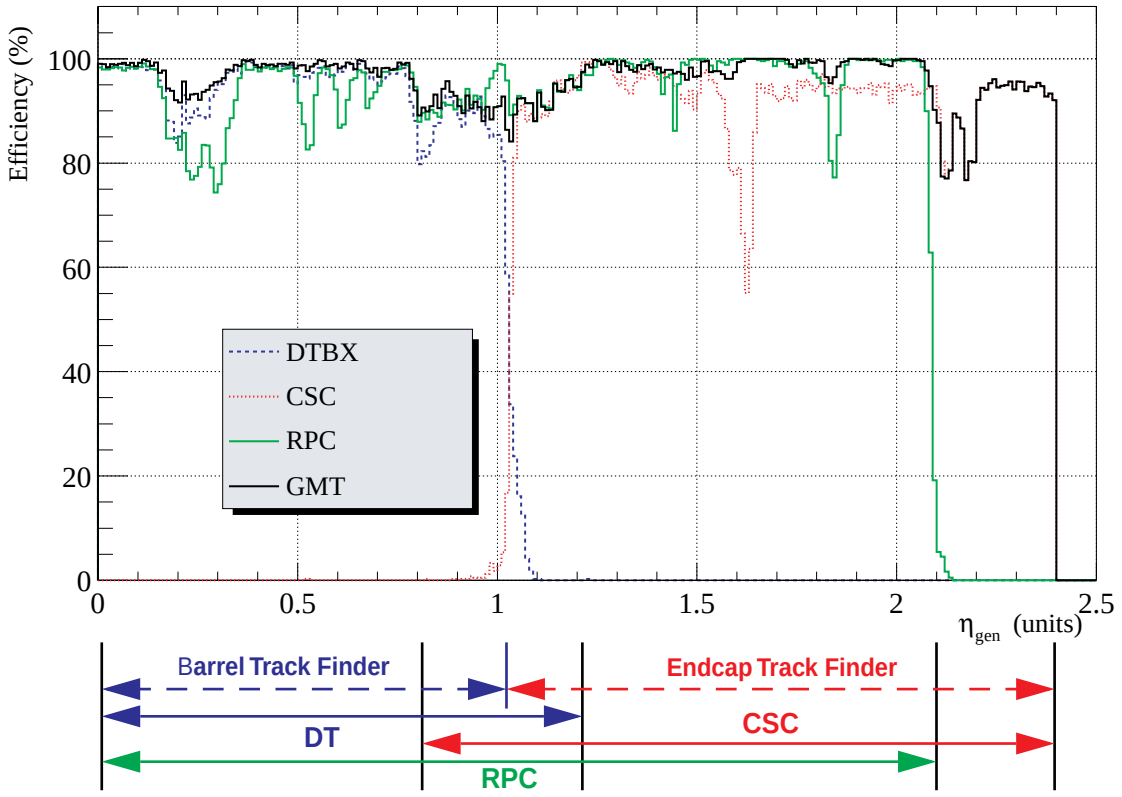

Fig. 8.18: Muon trigger efficiency vs η.

Trigger rates coming from various physics channels are shown in Fig. 8.19. Output rate can be adjusted to a desired value by changing the p_T threshold. Proposed values are given in Table 8.3.

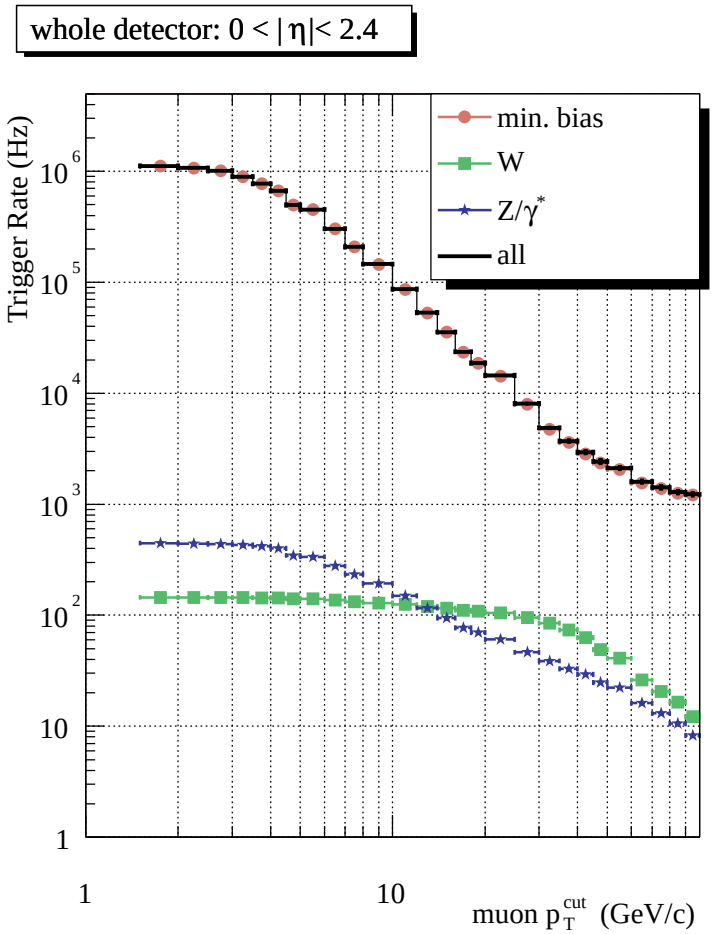

Fig. 8.19: Single muon trigger rate vs p_T threshold.

Table 8.3: Muon trigger thresholds and rates.

luminosity	10^{33} cm^{-2} s^{-1}			10^{34} cm^{-2} s^{-1}		
trigger	1μ	1μ +X	2μ	1μ	1μ +X	2μ
threshold [GeV/c]	10	4	3, 3	25	5	8, 5
rate [kHz]	8.7	2.2	1.5	8.1	2.4	2.8

In order to maximize the physics potential of the detector, the trigger thresholds should be lower than the corresponding off-line cuts. From Table 8.4 one can see that this criterion is fulfilled with large safety margin. The only exception is b-quark physics, because the rate of b-quark production is ~5 MHz and one can afford to take only a small fraction of events. However, one can devote some fraction of bandwidth to exclusive channels and thus enable to exploit the

lowest possible p_T thresholds. For other physics the 1μ trigger threshold is even lower than 1μ+X offline cut. This ensures very high efficiency for such triggers.

Table 8.4: Offline cuts on muons [GeV/c]

luminosity	10^{33} cm^{-2} s^{-1}			10^{34} cm^{-2} s^{-1}		
trigger	1μ	1μ +X	2μ	1μ	1μ +X	2μ
SM higgs	—	20	10, 5	—	20	20, 10
SUSY higgs	10	7	5, 5	—	20	10, 10
sparticles	—	10	10, 10	—	20	15, 15
exotica	—	100	20, 20	100	100	20, 20
top	50	50	30, 4	50	30	15, 4, 4
beauty	10	2-4	2-4, 2-4	—	—	—

8.5 Muon Trigger for Heavy Ion Runs

8.5.1 Low Momentum Threshold

Low p_T threshold is crucial for quarkonia detection. Its value should be limited only by the muon energy loss in calorimeters. The minimal value of the trigger threshold p_T^{min} is plotted in Fig. 8.20 as a function of $|\eta|$. Because of Landau fluctuations of the energy lost by muons, different p_T^{min} values are obtained for different required efficiencies ε. For comparison the total momentum p^{min} is also plotted. The error bars on the plots correspond to uncertainty of absorber distribution of one nuclear interaction length λ. One can see that in the barrel one can achieve $p_T^{min} \approx 4$ GeV/c for $\varepsilon = 90$ % or $p_T^{min} \approx 3.5$ GeV/c for $\varepsilon = 80$ %, where ε is the single muon trigger efficiency. In the endcap it decreases below 2 GeV/c. This allows us to explore central Υ, Υ', Υ''$\rightarrow \mu^+\mu^-$ production with good statistics at all p_T(Υ), down to p_T(Υ)=0.

Quarkonia decay in muon pairs. Efficiency for detecting both muons at L1 is rather low at low p_T. Triggering on anyone of the two muons would increase quarkonia efficiency significantly if the single muon L1 rate at the minimal threshold is acceptable. This is illustrated in Fig. 8.21.

8.5.2 Trigger Rates

In the case of heavy ion collisions the muon trigger rate is dominated by three major contributions:

- prompt muons (mainly from c- and b-quark decays),
- muons from hadron decays (mainly π and K),
- hadronic punch-through.

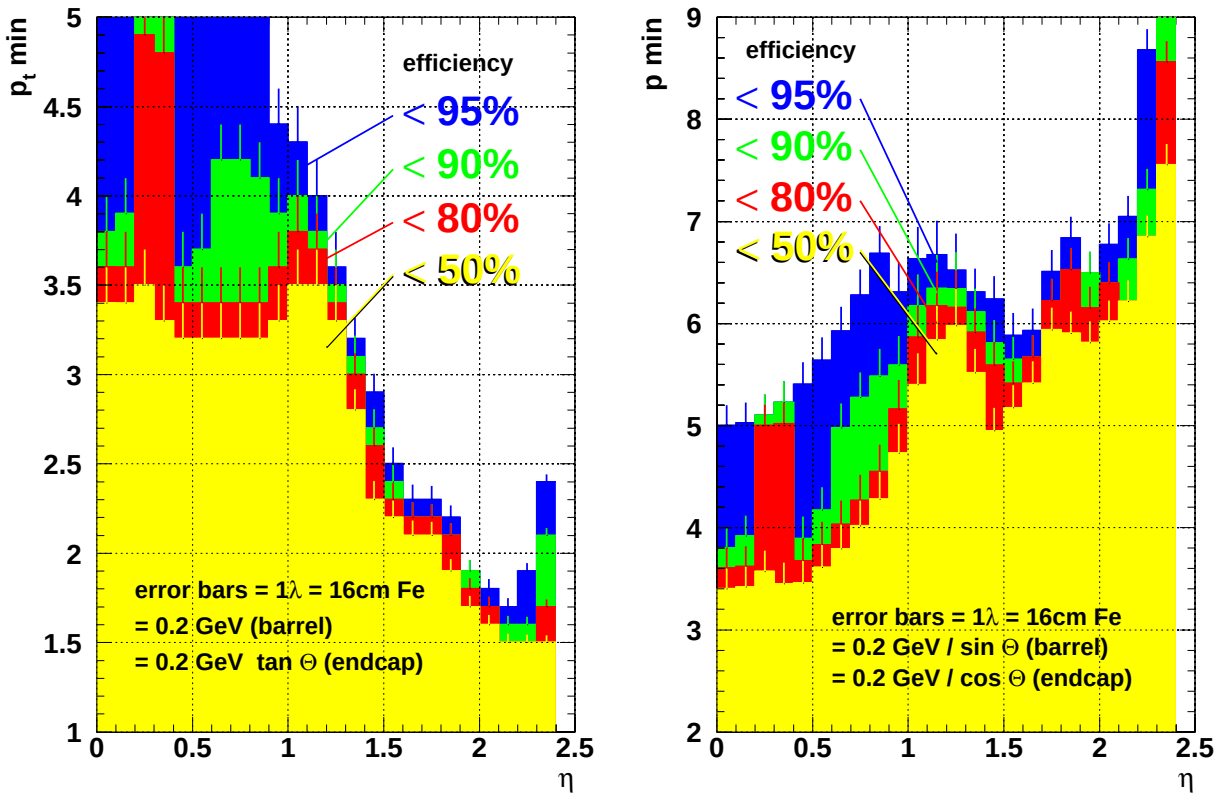

Fig. 8.20: Minimal muon trigger thresholds p_T^{min} and p^{min} for various required efficiencies as a function of muon pseudorapidity.

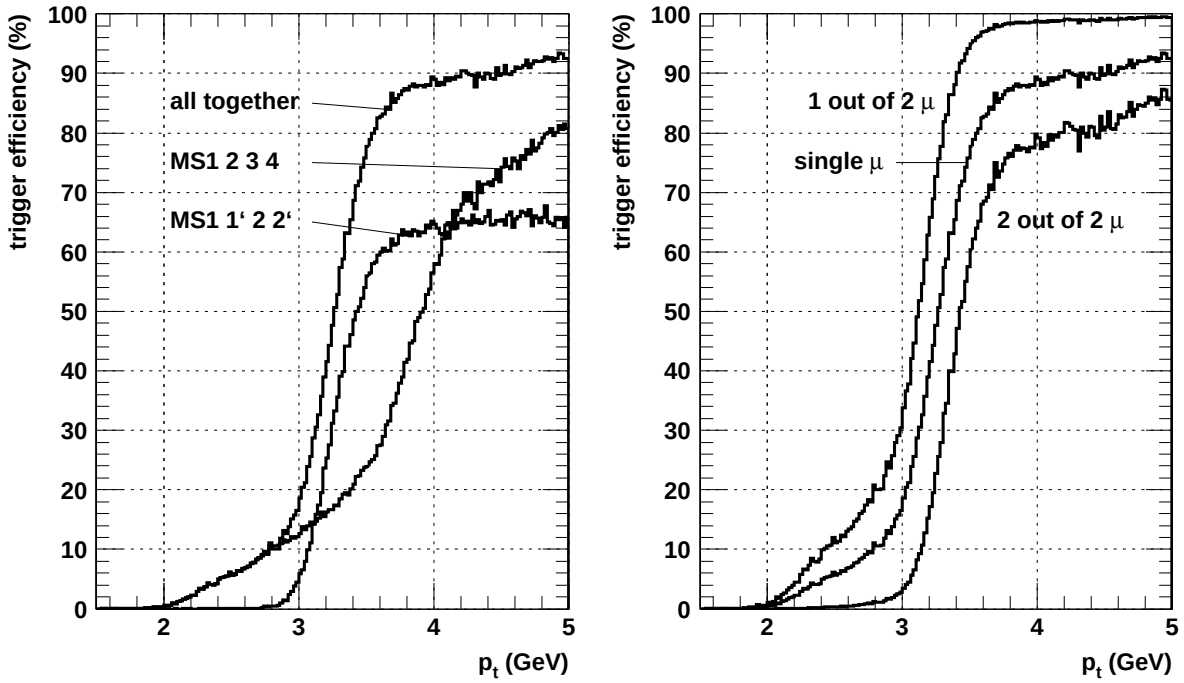

Fig. 8.21: Trigger efficiency in the case of 1- and 2-muon events ($|\eta| < 1.5$)

Detailed simulation has been performed [8.20] in order to evaluate those rates in the case of minimum bias Pb-Pb collisions. Results are shown in Fig. 8.22 for the nominal luminosity of $10^{27}cm^{-2}s^{-1}$. In the pseudorapidity range of $|\eta| < 1.5$, useful for quarkonia study, one can expect a single muon trigger rate of ≈500 Hz with almost equal contributions from prompt muons (c- and b-quark decays) and from hadronic punch-through + decays. This is well below the 5 kHz limit imposed by the DAQ bandwidth (Sec. 2.5). It allows us to run requesting a single muon at the first level trigger, which ensure high efficiency for $\Upsilon \rightarrow \mu^+\mu^-$. The second muon could be requested at L2, which would reduce the rate down to 60 Hz — already acceptable for the mass storage. This strategy is summarized in Fig. 8.23.

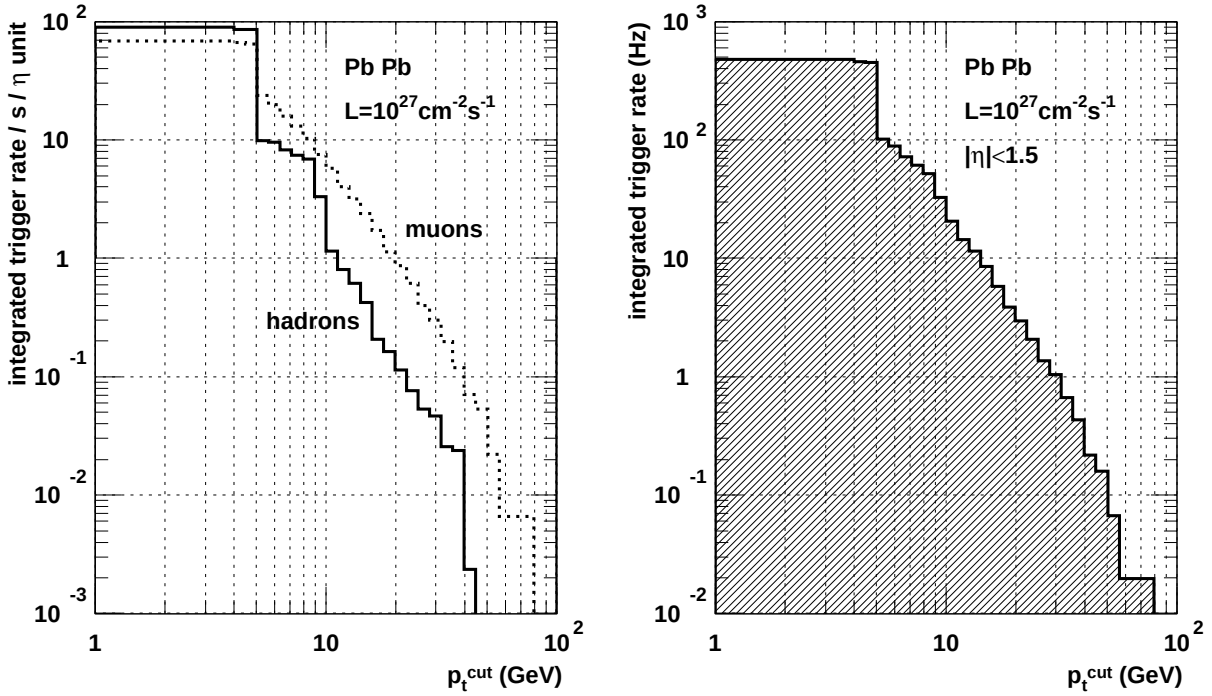

Fig. 8.22: Expected muon trigger rates for minimum bias Pb-Pb events.

The strategy described above works well for Pb-Pb collisions and it may work (with some modifications) in the Sn-Sn case. For lighter ions, however, the single muon rates are much higher (see Table 8.5) and one has to require two muons already at the first level. The price for this is an efficiency for low p_T muon pairs of 80% or even lower. Fortunately this is compensated by much higher luminosities which ensures to collect high enough statistics in spite of low efficiency.

Table 8.5: Single muon trigger rates for different ion species [8.20].

	pp	O O	Ar Ar	Kr Kr	Sn Sn	Pb Pb
luminosity [$cm^{-2}s^{-1}$]	10^{34}	$3.1 \cdot 10^{31}$	$1.0 \cdot 10^{30}$	$6.6 \cdot 10^{28}$	$1.7 \cdot 10^{28}$	10^{27}
1μ trigger rate [kHz]	190	120	21	5.7	2.9	0.5

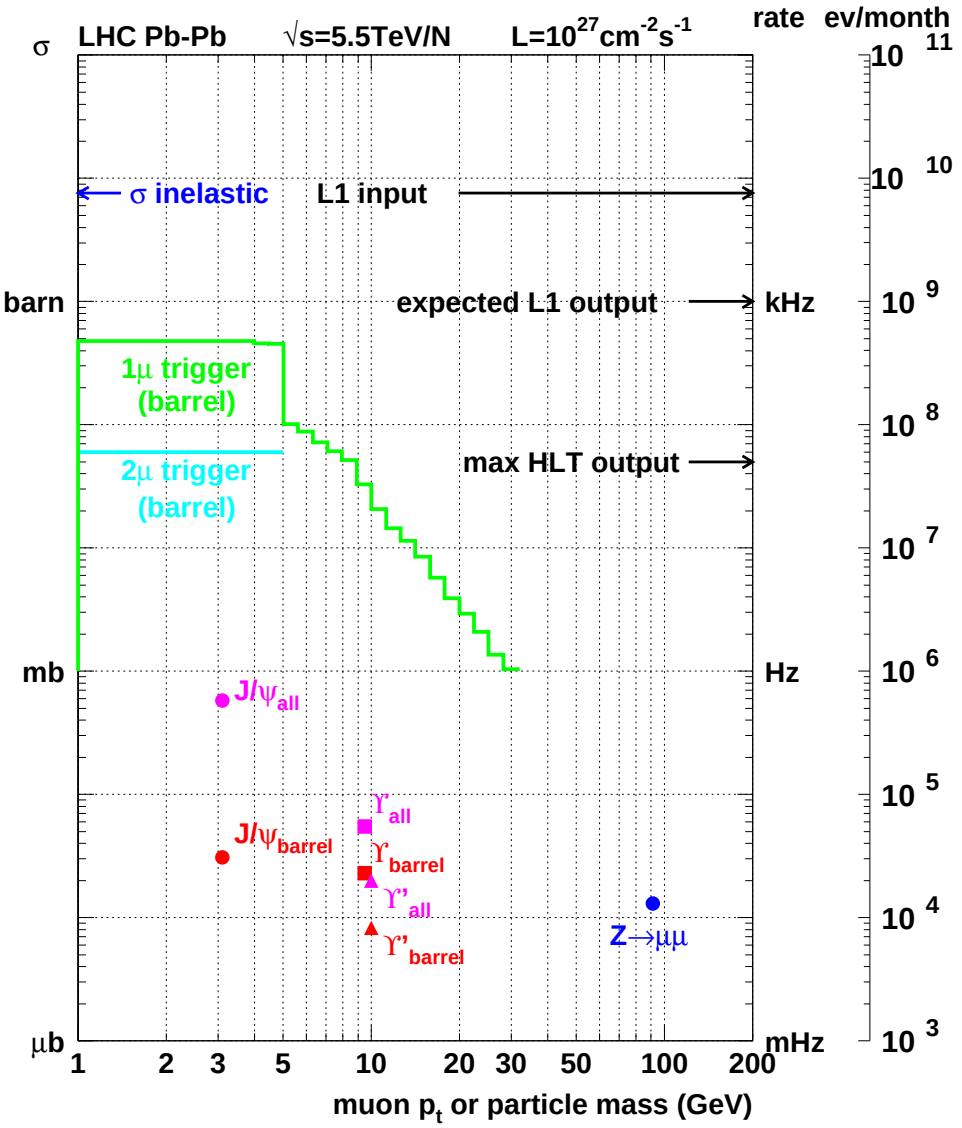

Fig. 8.23: Trigger and physics rates for minimum bias Pb-Pb events.

8.6 System robustness

Designing LHC detectors is a challenge in many aspects. The energy of collisions is an order of magnitude higher than in previous accelerators (TeVatron). Therefore there is significant uncertainty in the extrapolation of cross sections. Collision frequency is 4 times higher (HERA). High clock frequency might be a source of crosstalks. The 25 ns bunch spacing means that signals from different bunch crossings will be mixed in some detectors. The luminosity is ~10 times higher (TeVatron). This will cause a pileup of 10-20 pp interaction in a single bunch crossing. Radiation level will also be much higher than in previous experiments. Large multiplicities of particles implies fine granularity of detectors and hence huge number of channels. High energy of particles requires deep calorimeters and large tracking detectors with strong magnetic fields. Strong

radiation together with large size of detectors and huge amount of surrounding electronics cause access to the detector to be very limited. Some parts can be accessed only once a year for a short period. The situation becomes similar to experiments in space where there is no possibility to repair after the launch. On the other hand the huge amount of diverse electronics distributed over large area makes the LHC experiments not comparable to any other device. All those challenges requires very careful design in order to make the system robust.

Operation of the system can be distorted by two kinds of causes:

- bottlenecks within the system,
- malfunctioning of system elements.

A bottleneck could be a limited bandwidth, finite buffer size, finite two hit or two track resolution, etc. The size and frequency of errors caused by bottleneck depends mainly on the data stream itself, which is determined by

- signal physics (luminosity, correlations),
- background physics (in the case of muon detector it is punch-through, thermal neutrons, muon radiation, muons from the accelerator, etc.),
- state of the detector (pulse shapes, noise levels, timing, efficiencies, etc.).

Malfunctioning of system elements can be caused by external disturbances, like:

- electromagnetic disturbances (noise, crosstalk, RF, bad grounding, faulty power supply, etc.),
- radiation (radiation damage, single event upsets),
- temperature, humidity,
- mechanical stresses.

All those reasons can cause different kind of faults:

- transient (the data are distorted as long as the disturbance exists),
- permanent (the data are distorted until the system is reset),
- destructive (the element still work, but with lower performance),
- fatal (the element is faulty forever).

In order to limit the impact of all kind of failures each system should have the following features:

- redundancy,
- immunity to single, local failures (e.g. a single link should not serve > 1 % of a detector,
- possibility of (possibly remote) exchange of faulty element with a spare one,
- possibility of changing the algorithm (e.g. masking out noisy channel or requiring more stringent coincidence).

All those precautions are widely used in the CMS Muon Trigger System. First of all it consists of two complementary subsystems, DT/CSC and RPC, which can work independently. Within each subsystem the redundancy is provided by using four muon stations. In each station

there are 8-12 DT layers or 6 CSC layers. A brief summary of possible system bottlenecks and the tools to handle them is given in Tables 8.6 - 8.8. The second column of each table gives the location of each object abbreviated as follows: **D** - on the detector, **P** - on the periphery of the iron yoke, **C** - in the Counting Room. From the number of objects of each type one can judge what fraction of the detector is covered by a single object and how narrow is the bottleneck due to the bandwidth limit shown in the fourth column. The fifth column contains tools implemented to handle different kind of noise, including physics background and artefacts of the algorithms (e.g single track seen by two processors). In addition to the tools listed in the tables there is a possibility of masking out every channel at the input of each object. The last column tells what kind of redundancy is implemented in order to make the system immune against failure of the given object. This is usually provided by majority coincidences of M out of N elements, shortly denoted as “M/N”. For example a dead channel introduces local inefficiency in one layer, but the trigger is still efficient because of majority coincidence of 3/4 layers. The last column does not concern the Counting Room electronics, where a replacement can be done easily.

Table 8.6: Drift Tube Trigger chain

object	loc	quantity	bandwidth	noise handling	failure handling
channel	D	200 000	1 hit / bx	discrim. threshold	3/4 layers
BTI	D	50 000	1 track / bx	fit tolerance	1/2 superlayers
TRACO	D	4 400	2 tracks / 2 bx	matching tolerance	2/4 stations
Trigger Server	D	250	2 tracks / 2 bx	sorting priority	2/3 TSM chips
Sector Collector	P	60	2 tracks / 2 bx / station	output bandwidth = input bandwidth	several links
Track Assembler	C	72	2 tracks / 2 bx	matching tolerance, sorting priority	
Wedge Sorter	C	12	4 tracks / bx	quality threshold	
Barrel Sorter	C	1	4 tracks / bx	quality threshold	

All CMS muon trigger subsystems use discriminated detector signals, therefore the first line of defence against noise is obviously the discriminator threshold. In the case of Drift Tubes possible inefficiency due to dead or masked out channels is handled by the BTI making majority coincidence of hits in 3 out of 4 layers. Tolerance on this coincidence is programmable, so it can be tighten in case of high noise. Similarly TRACO has programmable tolerance on matching tracks from two superlayers, but also single (not matched) tracks can be accepted. Information about quality of coincidences in BTI and TRACO is sent to the Trigger Server which selects the 2 highest rank tracks per chamber. Since the rank is a programmable function of qualities and estimated p_T, it provides a powerful tool for background suppression. Because one Trigger Server covers the entire chamber, its potential failure could have relatively large impact on the system. Therefore it is made of 3 identical chips in such a way, that any two can serve the entire chamber. The last

critical element is Sector Collector providing the optical transmission to the Counting Room. It does not create any bandwidth bottleneck, so the noise is not an issue. However, its possible failure could affect an entire sector and therefore it is located in a more accessible place. Double background suppression is done at Track Assembler. First, the tolerance on matching track segments from different stations is programmable. Second, the priority of selecting 2 best tracks per 30° sector is a programmable function of p_T and matching quality. Also the final stages of sorting are based on programmable rank. In addition, low quality tracks can be removed from sorting.

In the case of CSC the redundancy is provided by majority coincidences of 2 out of 3 (or 4) muon stations and 4 out of 6 layers in each station. The Local Charge Tracks (LCT) are formed as patterns of hits in a given chamber. One can reduce background in a well controlled way by restricting the set of allowed patterns. If it is still too high one can accept only 5 out of 6 or 6 out of 6 coincidences. Further rate reduction is performed by Muon Port Card. It selects 2(3) highest quality track per 20° (60°) sector in ME1 (2,3,4). Again, the selection criteria are programmable. Track Finder processing is similar to that of DT. Track segments from different stations are matched to each other with programmable tolerance. Three highest rank candidates per sector are selected. Again, the rank is a programmable function of p_T and quality. This rank is also used for final sorting.

Table 8.7: CSC Trigger chain

object	loc	quantity	bandwidth	noise handling	failure handling
anode wire group	D	160 000	1 hit / bx	discrim. threshold	4/6 layers
cathode strip	D	200 000	1 hit / bx	discrim. threshold	4/6 layers
Anode LCT	D	432	2 tracks / bx	patterns, quality	2/3(4) stations
Cathode LCT	P	432	2 tracks / bx	patterns, quality	2/3(4) stations
Port Card ME1 ME2,3,4	P P	36 3×12	2 tracks / bx 3 tracks / bx	sorting priority sorting priority	2/3(4) stations 2/3(4) stations
Sector Processor	C	12	3 tracks / bx	matching tolerance, sorting priority	
Muon Sorter	C	1	4 tracks / bx	sorting priority	

The case of RPC Trigger is somewhat different as it does not have the intermediate step of forming tracks in single stations. On the other hand very good time resolution permits some background reduction by narrowing the input gate. The next step is already using the data from all stations. The tracks are formed comparing observed hits with preprogrammed patterns. Like in the case of CSC, careful pattern selection and quality tagging are powerful tools for background suppression. The final sorting is similar to that of DT and CSC.

The last but not least line of defence against background is at the Global Muon Trigger. Its programmable logic permits very flexible use of quality information. Purity of the data can be

largely improved by matching muon candidates from DT/CSC and RPC subsystems. Overall efficiency can be increased by accepting candidates seen only in a single system. Accepting only high quality singles ensures that the purity is not compromised significantly. Details of the algorithm can be adjusted to the current situation (detector status, background rate) in each detector region.

Table 8.8: RPC Trigger chain

object	loc	quantity	bandwidth	noise handling	failure handling
RPC strip	D	200 000	1 hit / 4 bx	discrim. threshold, gate width	3/4 stations
Master Link Board	P	732	8 groups × 12 strips / 8 bx		3/4 stations
Pattern Comparator	C	4752	1 track / bx	patterns, quality	
Trigger Board	C	396	4 tracks / bx	sorting priority sorting priority	
Trigger Crate	C	33	4 tracks / bx	sorting priority	
Barrel Sorter Endcap Sorter	C C	1 1	4 tracks / bx 4 tracks / bx	sorting priority sorting priority	

The key ingredients implemented all the way through the trigger chain are quality information and programmable selection criteria (patterns, ranks, etc.). Wherever possible explicit cuts are avoided in favor of sorting and selection. This makes possible tuning of the algorithms to a very wide range of conditions. High redundancy and flexibility of the algorithms is what makes the CMS Muon Trigger a very robust system.

References

[8.1] CMS Muon Technical Design Report, **CERN/LHCC 97-32**, 1997.

[8.2] M. Benettoni et al., Nucl. Instr. and Meth **A 410** (1998) 133.

[8.3] M. Aguilar-Benitez et al., Nucl. Instr. and Meth **A 416** (1998) 243.

[8.4] F. Gasparini et al, Nucl. Instr. and Meth **A 336** (1993) 91.

[8.5] A. Kluge, T. Wildschek, **CMS Note 1997/091**.

[8.6] A. Kluge, T. Wildschek, **CMS Note 1997/092**.

[8.7] A. Kluge, T. Wildschek, **CMS Note 1997/093**.

[8.8] G. M. Dallavalle et al, **CMS Note 1998/042**.

[8.9] M. Kloimwieder, **CMS Note 1999/054**.

[8.10] M. Andlinger et al., Nucl. Instr.and Meth. **A 370**, 389, (1996).

[8.11] T. Sjostrand et al., *High Energy Physics Event Generation with PYTHIA 6.1*, **hep-ph/0010017**, LU TP 00-30; T. Sjostrand, Computer Physics Commun. **101** (1997) 232.

[8.12] N. Neumeister et al., *Monte Carlo simulation for High Level Trigger studies in single and di-muon topologies*, **CMS IN 2000/053**.

[8.13] CMS Simulation Package CMSIM — Users' Guide and Reference Manual, http://cmsdoc.cern.ch/cmsim/cmsim.html

[8.14] *GEANT - Detector Description and Simulation Tool*, CERN Program Library Long Writeup **W5013**.

[8.15] P.A. Aarnio et al., *FLUKA86 user's guide*, CERN TIS-RP/168 (1986);
P. A. Aarnio et al., *Enhancements to the FLUKA86 program (FLUKA87)* CERNTIS-RP/190 (1987), A. Fass` o et al, *FLUKA: present status and future developments*, Proc IV Int. Conf. on Calorimetry in High Energy Physics, La Biodola, Sept 20-25, 1993, Ed. A. Menzione and A. Scribano, World Scientific, p. 493 (1993);
A. Fass` o et al., *FLUKA: performances and applications in the intermediate energy range*, Special-ists' Meeting on Shielding Aspects of Accelerators, Targets and Irradiation Facilities, Arlington, Texas, April 28-29, 1994.

[8.16] CMS Reconstruction Software: The ORCA Project, **CMS IN-1999/035**.

[8.17] *Status Report of the RD5 Experiment*, **CERN-DRDC/93-49**;
C. Albajar et al, Z.Phys. **C 69** (1996) 415;
C. Albajar et al, Nucl. Instr. and Meth **A 386** (1997) 421.

[8.18] M. Huhtinen, *Optimization of the CMS forward shielding*, **CMS Note 2000/068**.

[8.19] C. Albajar and G. Wrochna, *Isolated Muon Trigger*, **CMS Note 2000/067**.

[8.20] G. Wrochna, **CMS Note 1997/089**.